Environmental
Studies
Research
Fund

213

Development, Validation and Implementation of an Operational Ocean Forecasting System for the Grand Banks And Orphan Basin for Daily Operational Delivery at the Canadian Meteorological Centre

Développement, Validation et Implémentation d’un système de prévision océanique pour les Grands Bancs et le Bassin Orphan pour livraison journalière au Centre Météorologique Canadien

Canada 2019

Development, Validation and Implementation of an Operational Ocean Forecasting System for the Grand Banks and Orphan Basin for Daily Operational Delivery at the Canadian Meteorological Centre

Développent, Validation et Implémentation d'un système de prévision océanique pour les Grands Bancs et le Bassin Orphan pour livraison journalière au Centre Météorologique Canadien

Prepared for

Environmental Studies Research Funds

By

F.J.M. Davidson, G.C. Smith, Y. Lu, V. Bouchet, A. Methot, J. Lei, L. Zhai, J. Xu, G. Holden, F. Dupont, S. Higginson, W. Yu, P. Pellerin

F.J.M. Davidson

Fisheries and Oceans Canada

80 East Whitehills Road.

P.O. Box 5667

St. John's NL

Canada A1C 5X1

Contents

ABSTRACT

Oil industry operations for the Grand Banks and those proposed for the Orphan Basin are vulnerable because presently available sparse in-situ and remotely sensed oceanographic data in the region are not exploited to their full potential to provide oceanographic assessments and forecasts in the region. This report covers the development to implement a Canadian east coast operational coupled ocean and ice forecast system capable of ingesting the vast quantities of available operational satellite data and limited in-situ data for the region to provide reliable assessed and forecast currents any ocean depth.

This report covers the development and implementation of an ocean and ice forecasting system for the Canadian east coast capable of integrating the vast quantities of available operational satellite data and limited in-situ data and provide reliable assessment and forecast of currents at any ocean depth. The operational forecast output is made available for interested third parties to: run iceberg drift predictions; to run oil spill scenario tests; environmental characterisation for environmental assessments, strategic planning and operations; and if ever needed to run oil spill drift and fate predictions for environmental response.

Overall this project enables an increase in resolution of the ocean forecast model for the east coast along with improving initial conditions for the forecast system. The model output will increase the realism of drift prediction scenarios for the east coast of Canada.

SOMMAIRE

Les activités pétrolières dans les Grands Bancs et celles proposées dans le bassin Orphan sont vulnérables car les données océanographiques in situ sont rares et les données par télédétection disponibles ne sont pas pleinement exploitées pour fournir le maximum d'information sur l'état de l'océan et des prévisions océanographiques dans la région. Ce rapport couvre le développement et la mise en place d'un système de prévision des glaces et des océans sur la côte est du Canada, capable d'intégrer une vaste quantité de données satellitaires disponibles et le peu de données in situ disponibles dans la région afin d'estimer et de prévoir la circulation océanique sur toute la profondeur.

Ce rapport couvre les améliorations du modèle océanique, les améliorations des conditions initiales pour la prévision, le system d'évaluation des prévisions, la transition aux opérations ainsi que les efforts de dissémination des produits opérationnels au Centre de Prévision Météorologique et Environnemental.

Les sorties de prévision sont mises à la disposition des tierces parties pour: prévoir les trajectoires d'icebergs; exécuter des tests de scénario de déversement d'hydrocarbures; la caractérisation de l'environnement pour les évaluations environnementales, pour les plans stratégiques et les opérationnels; et, si besoin est, de faire des prévisions sur la dérive des hydrocarbures et sur leur devenir en vue d'une intervention environnementale.

En bref, ce projet permet d'accroître la résolution spatiale du système de prévisions des océans pour la côte est et d'améliorer les conditions initiales du système de prévision. Les résultats du modèle augmenteront le réalisme des scénarios de prévision de la dérive sur la côte est du Canada.

INTRODUCTION

This project was carried out by Environment and Climate Change Canada (ECCC) and Fisheries and Oceans Canada (DFO). These organizations are united under a tri-departmental initiative together with the Department of National Defense (DND) entitled Canadian Operational Network of Coupled Environmental PredicTion Systems (CONCEPTS). CONCEPTS activities are designed to build a Canadian operational coupled atmosphere-ocean-ice prediction capacity. Here the emphasis is on operational oceanography. This project delivers a state-of-the-art operational ocean forecasting prediction system for the Canadian east coast and initiates the long term provision of routine core ocean prediction service by the Canadian Government for the region. This project enhances the Canadian oil industry supply sector's ability to provide reliable applied oceanography and meteorological based products and advice, for oil spill drift scenarios, environmental assessments or routine operational decisions at sea on the Canadian east coast.

The two project objectives are:

1. Implement a validated operational ocean forecasting system for the Newfoundland Grand Banks and Orphan Basin region at the Canadian Centre for Meteorological and Environmental Prediction (CCMEP; formerly Canadian Meteorological Centre) and
2. Provide routine operational ocean current prediction output on a data server for third parties to recover and use for oil spill prediction/mitigation and other environmental assessment applications.

The tasks to achieve this were as follows:

Task 1: Development and improvement of a high-resolution (~2.5km) ocean forecast model over the Grand Banks. A regional high-resolution configuration for the Grand Banks and Orphan Basin will be added to the suite of ocean forecast systems used in CONCEPTS with a horizontal resolution around 2.5 km (or 1/36° latitude/longitude) covering a square domain of 1000 km by 1000 km. This high-resolution configuration is nested in the regional CONCEPTS MET/NAVAREA ocean forecasting system covering the Arctic and North Atlantic at 1/12° resolution.

Task 2: Improvement of analysis for initial conditions of ocean forecast: This task used as starting point the METAREA and BREA project analysis tools as they became available. The objective here is to pay specific attention to improving analysis for the Grand Banks and Orphan Basin region by adjusting the assimilation to finer scales. Improvements will include using a more accurate mean dynamic topography (MDT) in the assimilation of sea level anomaly as well as using new expected sea level anomaly data. A new higher-resolution MDT product has been developed (REF 3) that shows significant improvements over the Grand Banks. This MDT will be integrated into the assimilation system and the resulting impact on analysis quality and forecast skill will be investigated.

Task 3: Validation: An intensive evaluation of currents from model hindcasts were made with ocean observations (moorings, drifters), allowing a detailed assessment of model skill and permitting further improvements. Collaboration with project by Greenan et al.[1] will occur here for the Sackville Spur Area.

Additionally, this task developed a set of validation protocols to quantify the skill of forecasts of currents. The final deliverable for this task is a document describing the validation protocols and the specific techniques/calculations necessary to perform them as well as ongoing validation output. This task was complemented by the development of the Ocean Navigator (http://navigator.oceansdata.ca), an intuitive browser based web interface where verification and other features of the ocean prediction output can be accessed and displayed.

Task 4: Implementation of forecast system to operations: The development of proper interfaces and links for operational execution of the high-resolution hydrodynamic model at CCMEP were addressed. In order for systems to be run operationally at CCMEP, they must be re-written in specific software used by the operations at CCMEP. This software controls the sequencing of the various operational suites running at CCMEP and allows operators to quickly detect and correct errors as they occur to maintain the reliability of the systems.

[1] https://www.esrfunds.org/sites/www.esrfunds.org/files/publications/ESRF202-Greenan-et-al.pdf

Task 5: Implementation of an operational dissemination system: Development and implementation of operational provision of ocean forecast data through the Meteorological Service of Canada (MSC) Datamart (the web location where ECCC makes their forecast products available) will initiated. End user interaction will be actively pursued to ensure ocean forecast products are accessed correctly from MSC Datamart. Furthermore the development of simple web visualization of ocean forecast data for industry and public will occur in this task.

Additionally, this task included the development of the Ocean Navigator, which is a prototype web interface developed in the final year of this ESRF project to improve the uptake and use of Ocean Forecast output by the oil industry.

In the following report we review in plain language what has been achieved for each task, including any additional work/deliverables achieved beyond the initial project scope. We then cover industry engagement and provide an update for the roll out of the operational ocean forecasting system as well as a future outlook on potential applications by industry of this project. The plain language report for each task is complemented by a more technical appendix description of the activity done in the task.

Plain language task report and achievements

Task 1: Development and improvement of a high-resolution (~2.5km) ocean forecast model over the Grand Banks.

A model configuration using the NEMO (Nucleus for European Modelling of the Ocean) ocean model numerical code with 1/36° resolution was set up for the Grand Banks of Newfoundland and the adjacent waters. The model was tuned with numerous hindcasts (multi-year model simulations to test numerical model) to ensure use of the right model parameters such as diffusivity and friction over the bottom. With an increase in resolution, model parameterization need to be verified and adjusted to get the right results. Additionally the tidal forcing, boundary conditions and model parameters were tuned to get the tidal signal right in the domain.

A 3-year hindcast using NEMO version 3.6 was done on the domain as well as a 4-year hindcast using the older NEMO version 3.1. These hindcast runs allowed further tuning of the model as well as verification of model results against satellite observation. Results are available in appendix A. Comparisons between the new fine-scale 2-km resolution model and existing 7-km resolution model were done. An interesting output is that mean kinetic energy in the model decreases with higher resolution, but that eddy kinetic energy (i.e. the variable component) increases hinting at weaker mean flows, but stronger variable flows.

Task 2: Improvement of analysis for initial conditions of ocean forecasts

Two approaches to produce ocean state estimates are used in this project. The first, involves integrating all available ocean observations with a numerical estimate of the ocean state using a least-squares fit based on the relative error of the model and observations; a process referred to as “data assimilation”. This approach follows closely what is used in numerical weather prediction. A second approach is used to generate high-resolution (kilometer-scale) initial conditions where sufficient observations are not available to adequately constrain the small scales. For this, the high-resolution model is nudged towards the lower-

resolution analyses produced using data assimilation, in such a way that avoids damping of small-scale processes. These small scales are generated by the high-resolution ocean model based on the representation of the coastal processes (e.g. due to bathymetry and tides). In this way the large-scale ocean state can be "downscaled" to include the details from the coastal ocean model while maintaining the larger-scale ocean state in the coarser resolution data assimilative model.

In this section, the work to improve both these aspects is presented. First, the improvements to the SAM2 (System d'Assimilation Mercator) data assimilation system used in the Global Ice Ocean Prediction System (GIOPS) is presented. These improvements have now been incorporated in the operational system running at CCMEP called GIOPSv2.1. Second, the spectral nudging approach developed to initialize the high-resolution system for the Grand Banks is presented. The details of this are in Annex B.

Task 3: Validation

In this task we verified forecast accuracy by comparing ocean model prediction output against available observations. This approach is referred to here as producing "Class 4" metrics, following standards developed by the international ocean forecasting community. The term Class 4 refers to the method where model output is interpolated to the time and spatial location of the observation for direct comparison (see Hernandez et al 2015). Performance was evaluated for several parameters including temperature, salinity, sea level anomaly, and sea ice total concentration. This type of comparison is used by the international community and provides an objective way to compare systems and provide a quantitative assessment. The focus initially was on the evaluation of temperature and salinity. With a lack of in-situ observations to verify the model throughout an entire year, the project deployed 50 surface-drogued drifters on the Newfoundland and Labrador (NL) shelves as well as upstream. This provided additional temperature verification, but also velocity verification capacity for the ocean prediction systems.

In this task, verification tools and protocols were developed and tested on the GIOPS prediction system, but are transferable to the high-resolution shelf prediction systems developed in this project. See Annex 3 for further details.

Task 4: Implementation of forecast system to operations:

A high-resolution (1/36°) NEMO-CICE ocean forecast maestro suite of Grand Banks region (GBN) has been set up on ECCC super-computer network, based on the domain configuration of Task #1. The ocean configuration is referred to as Grand Banks 1/36° resolution (GBN36), and the forecasting system using this configuration will be called the Coastal Ice Ocean Prediction System (CIOPS). A 3-month simulation for 2014 summer (June 1st to August 31st) was carried out with this configuration to test the capability of this model in a user account. The high-resolution model showed the ability to create higher-temperature gradients than the coarser larger-scale models, indicating it can produce high-level details of ocean circulation. This task provided a full operational simulation over a 3-month period of the high-resolution coastal prediction system for the Grand Banks.

Task 5: Implementation of operational dissemination system

The MSC Datamart is the real-time data dissemination repository operated by CCMEP that contains data up to five days in the past from the various operational meteorological and environmental prediction systems. The MSC Datamart is publically accessible and accessed by a number of real-time end users. The repository is: http://dd.weather.gc.ca/about_dd_apropos.txt and an efficient protocol for retrieval (AMQP) can be retrieved from: http://dd.weather.gc.ca/doc/README_AMQP.txt

This project focused on the delivery of a high-resolution forecast system to operations at CCMEP. This task implemented ocean forecast provision on the MSC Datamart. Development of the delivery of the CONCEPTS GIOPS products to the MSC Datamart paved the way for the delivery of the CONCEPTS Regional Ice Ocean Prediction System (RIOPS). For this project, this will lead to the delivery of a high-resolution 2 km ocean ice forecast system covering the Grand Banks and Orphan Basin on the MSC Datamart (expected in early 2019).

To complement an online real-time archive, visualisation and discovery systems are needed. Within this project, it was realised there would be very little use of the project's forecast system output if there was no reasonable mechanism to explore, discover and evaluate it. Since April 2016, the final year of the project, the Ocean Navigator web (API) server was developed (accessible at http://navigator.oceansdata.ca).

Ocean Navigator

The Ocean Navigator developed within this project is a visualisation and discovery tool that interprets end user commands to access specific portions of the raw NetCDF-4 output archive and transforms it on the fly into a suite of different plots for visualisation, verification and statistics extraction. Both derived data and plots can be saved. The tool is currently accessible from http://navigator.oceansdata.ca and is situated on a computer hosted by the Marine Environmental Observation Prediction and Response Network (MEOPAR) at the Dalhousie University campus. The Ocean Navigator tool has a broad range of applications by physical oceanographers, marine biologists, industry, academics and the public for a variety of end uses ranging from simple to sophisticated demands. The Navigator type approach permits a customized approach to visualising data, as it access the raw output in NetCDF-4 and produces any derived products on the fly. Additionally it can view Class 4 verification files, as well as perform inter-comparisons with observations and other forecast systems. Such a product was needed to get more usage out of the ice ocean forecast products, in particular by industry.

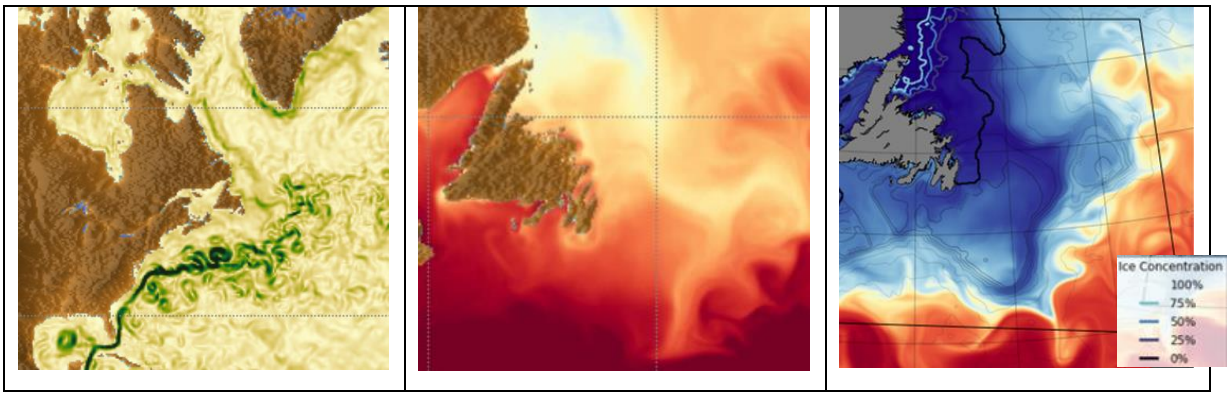

Figure 1: *Example of output from Ocean Navigator tool for regional and global forecast systems. Left panel: currents; Middle panel: summer-time temperature; Right panel: winter-time temperature with contours of sea ice concentration.*

At present, the Ocean Navigator tool has been developed as a prototype to help disseminate the work and forecast systems created under this ESRF project. It will be a tool made available to the CONCEPTS DFO service desk that will commence to be staffed in 2017-2018 at ECCC-CCMEP in Dorval. This tool will help the service desk assist end users of the ocean forecast system to find the right data for their needs. It will also permit the service desk to set up customized derived products for particular events and locations very quickly as well as automate any routine visualisation products needed.

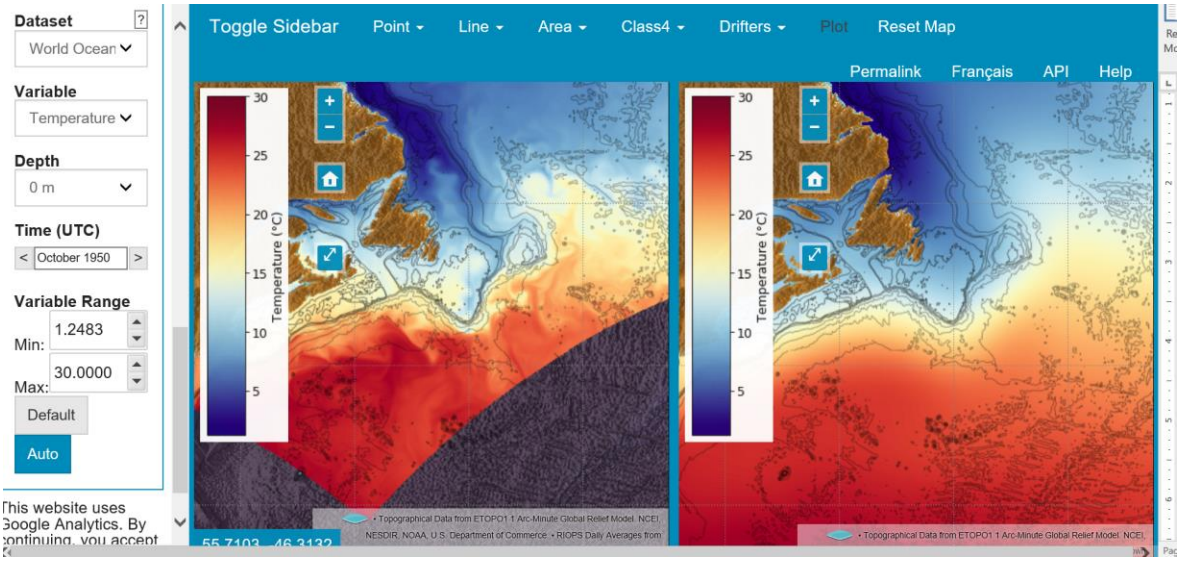

Figure 2: *Example of output from Ocean Navigator tool for regional and global forecast systems.*

Furthermore, a link is provided in Annex E for the Ocean Navigator user's manual as well as the code repository for the Navigator on GitHub.

Summary / Outlook

In this project we have created a high-resolution ocean prediction system now called CIOPS for the Grand Banks and adjacent waters. This prediction system is designed to run daily at the ECCC CCMEP. The implementation and availability of the products from this ocean prediction system is anticipated for Spring 2019. The project has developed all the necessary

tools for initialisation of forecast, visualisation, accessibility, verification and implementation for this high resolution ocean ice prediction system, and implanted/tested these on GIOPS and RIOPS.

Finally, this project benefitted from stakeholder participation that occurred through regular TAG committee meetings as well as an industry interface meeting in May 2015**.** An additional stakeholder meeting is envisioned prior to the final roll out of the high-resolution east coast forecasting systems developed in this project in early 2019.

Annex A

Task 1: Development and improvement of a high-resolution (~2.5km) ocean forecast model over the Grand Banks.

Overview

The model developed in this project covers the region around the Grand Banks of Newfoundland, thus denoted as GBN36. It is based on two versions (3.1 & 3.6) of the Nucleus European Modelling of the Ocean (NEMO, https://www.nemo-ocean.eu), with major difference between the two versions described below.

Model domain covers the region around the Grand Banks of Newfoundland with a nominal horizontal resolution of 1/36° in longitude/latitude. Horizontal grids follow the tri-polar ORCA configuration (Drakkar Group, 2007), with an average grid spacing of 2.2 km in the model domain. The vertical grid has 50 z-levels, in full cell sizes in the water column and partial cell size near the bottom. The full cell sizes vary from 1 m at the surface to 450 m at 5000 m. There are 23, 27 and 32 levels for the upper 100 m, 200 m and 500 m, respectively. The maximum and minimum water depths are 5275 m and 3.8 m.

A large number of tests have been carried to determine the model parameters related to sub-grid scale mixing. The vertical eddy diffusivity for tracers (temperature and salinity) and viscosity for momentum are computed using GLS (General Length Scale; Umlauf and Burchard, 2003). The bottom friction is parameterized using a non-linear quadratic law, with a fixed drag coefficient of 5×10^{-3}. The horizontal mixing of tracers is parameterized by a Laplacian scheme along isopycnal levels with the eddy diffusivity set to be 10 $m^2\ s^{-1}$. For the parameterization of horizontal mixing of momentum, both bi-Laplacian and Laplacian schemes have been tested. In the case of bi-Laplacian scheme, the viscosity varies spatially with the cube of the horizontal grid spacing according to $-A_M(\frac{\Delta x}{\Delta xm})^3$, where Δx and Δx_m are the averaged local and maximum grid spacing, respectively. In the case of Laplacian scheme, the horizontal viscosity is computed according to the Smagorinski scheme that relates the magnitude of viscosity coefficient to the strength of horizontal shear of the velocity.

The two versions of the model use different values for horizontal viscosity. For the version based on NEMO v3.1, A_M is set to be 10^9 m^4 s^{-1}. Further reducing this parameter to 10^8 m^4 s^{-1} led to a numerical instability as described by Zhai et al. (2015), that is referred to as the "Hollingsworth instability" (Hollingsworth et al., 1983). This numerical issue is fixed in NEMO v3.6 (Ducousso & Madec, 2015), which allows using $A_M = 10^8$ m^4 s^{-1}, leading to about 10% increase of domain-averaged kinetic energy than using $A_M = 10^9$ m^4 s^{-1}. It is worth noting that using $A_M = 10^9$ m^4 s^{-1} the two versions of the model obtain very similar solutions.

The sea-ice module is turned off because seasonal sea-ice only develops near the coast in the model domain. Sea surface temperature (SST) below freezing point is set to be the freezing temperature. The model obtains accurate solution of tidal elevation when tidal forcing is included in model's lateral boundary condition. However, tidal influences on the sub-tidal circulation and temperature/salinity distribution are not significant. Hence, tides are not included in all tests.

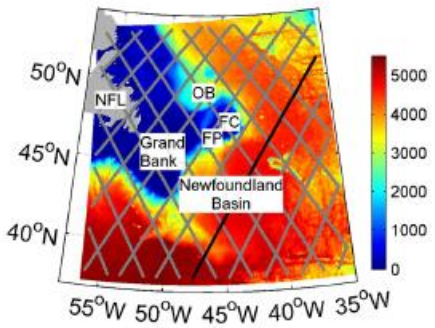

Figure 3: *Bottom topography (m) and model domain of GBN36, overlaid with satellite altimetry ground tracks. The track highlighted in bold black is used for spectral analysis. Abbreviations: FC Flemish cap, FP Flemish Pass, NFL Newfoundland, OB Orphan Basin.*

Model bathymetry is the block-median of SRTM30_Plus, the global bathymetry and elevation data at 30 arc seconds resolution (Becker et al., 2009). SRTM30_Plus compiled 298 million edited soundings and used them to modify global satellite bathymetry based on the latest altimeter-derived gravity models.

At open boundaries, barotropic (depth-averaged) and the remaining baroclinic components of horizontal velocities are treated differently. The radiation condition of Flather

(1976) is applied to the modelled barotropic velocity normal to a lateral open boundary based on the prescribed barotropic velocity and the difference between the prescribed and modelled SSH. The relaxation zones of 10-grids are applied to the baroclinic velocity and T/S at the open boundary with a relaxation parameter varying between 0 and 1 within the relaxation zones. In addition to this relaxiation, either the Orlanski forward implicit scheme (Marchesiello et al., 2001) or the flow relaxation scheme of Engedahl (1995) is applied.

The model's initial and lateral boundary conditions, as well surface atmospheric forcing, are obtained from different sources for different tests to be described separately in Annexes A.1.1 and A.1.2.

Part 1: A 4-year (2003-2006) hindcast with GBN36 based on NEMO v3.1

The first stage of the GBN36 development and evaluation are documented in Zhai et al. (2015). At this stage, GBN36 takes initial and lateral boundary condition from the CREG12 model covering the Arctic and North Atlantic (Dupont et al., 2015). The surface atmospheric forcing is the hourly field of the operational Global Deterministic Prediction System of the Canadian Meteorological Centre (Smith et al., 2013). A 4-year hindcast covering 2003-2006 is carried out. Here we provide a summary of key results.

a. Time-mean state

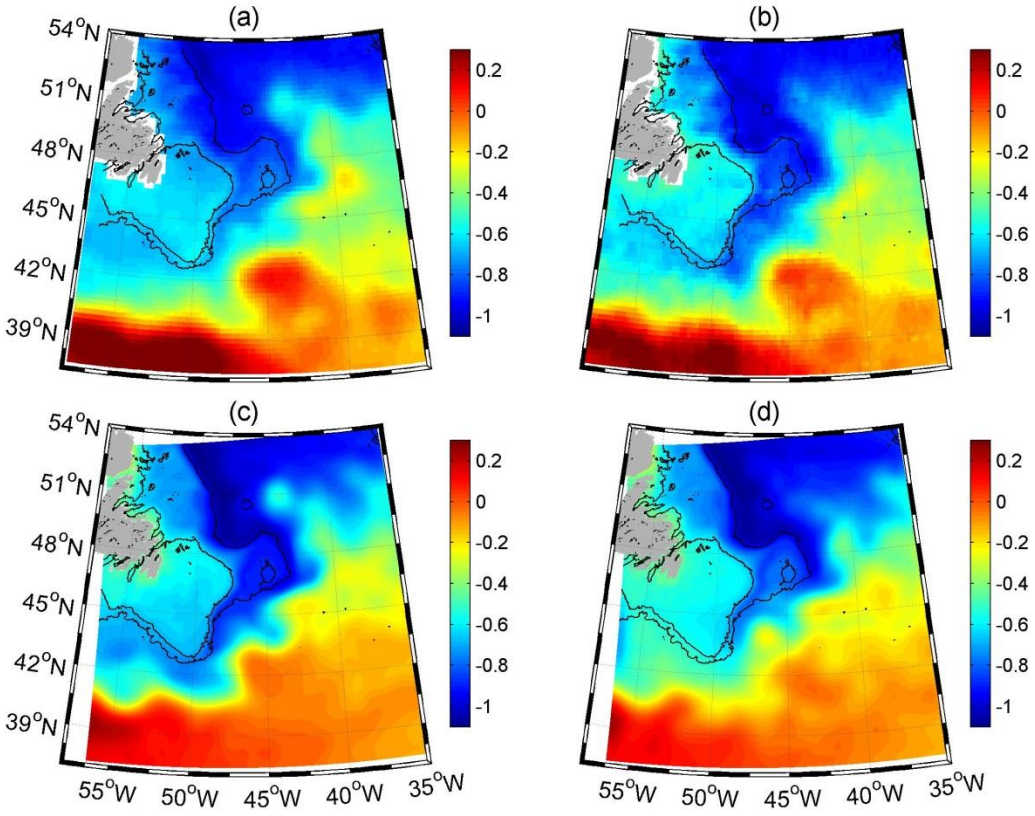

Figure 4: *Mean dynamic topography (MDT, in m), (a) distributed by AVISO and (b) derived in Higginson et al. (2011), referred to as MDT_G. Mean sea level computed by (c) CREG12 and (d) GBN36.*

Fig. 4 shows mean SSH from CREG12 and GBN36 as well as the mean dynamic topography (MDT) from AVISO and derived in Higginson et al. (2011). They all show sharp gradients to the east and northeast of the Grand Banks, low values in the Labrador Sea, and high values over the Gulf Stream. High values corresponding to cyclonic circulation around the Mann Eddy at 42° N and 44° W are evident. Overall the two MDTs are close to each other, and both show

differences with the modelled mean SSHs.

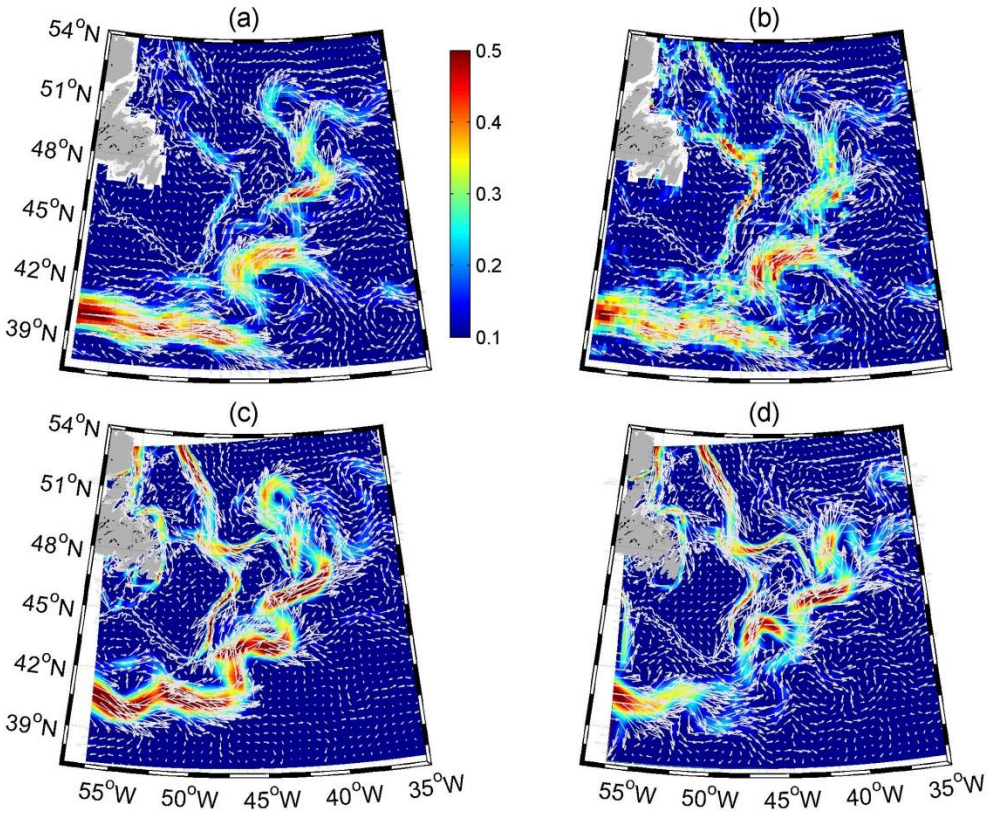

Figure 5: *Mean geostrophic currents derived from (a) AVISO MDT, (b) MDT_G, mean SSH of (c) CREG12 and (d) GBN36. Color shading shows speed in m s-1 and arrows show direction of currents.*

Fig. 5 shows the mean surface geostrophic currents computed from the MDTs and modeled mean SSHs. Fig. 5 shows mean surface velocity estimated from surface drifter observations and the two models. The similarity between Figs. 4 and 5 suggests that the mean surface circulation can be primarily accounted for by geostrophic currents. The circulation features derived from drifter data and observed MDTs are generally consistent. The eastward Gulf Stream centered around 40° N splits into two branches. One branch turns around the southeast Newfoundland Rise to flow northward into the Newfoundland Basin and becomes the NAC. The other branch turns southward around 46° W marking the return flow from the Gulf Stream into the Sargasso Sea. The Labrador Current has an inshore branch on the Labrador Shelf and around the Avalon Peninsula of Newfoundland, and two off-shore branches with one flowing southward through Flemish Pass and the other flowing eastward north of Flemish Cap. A portion of the Labrador

Current turns offshore at the Tail of the Grand Banks, mixes with water from the NAC, and then flows northward inshore of that current. Another part flows around the Tail of the Grand Banks.

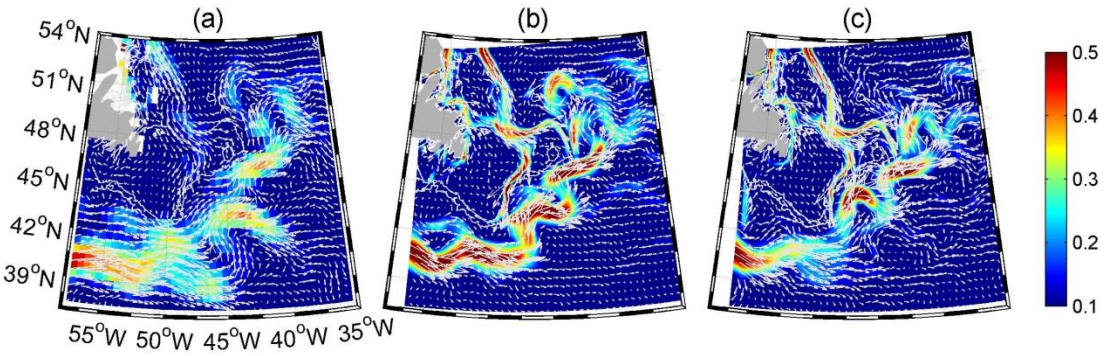

Figure 6: *Mean surface currents (a) derived from drifter data, and modelled by (b) CREG12 and (c) GBN36. Color shading shows speed in m* s^{-1} *and arrows show direction of currents*

The surface currents from the two models show agreement with those derived from MDTs and drifter data (Figs. 5 and 6). Both models produce stronger inshore and offshore branches of the Labrador Current than that derived from drifter and the MDT data. The position of the Gulf Stream crossing 55° W is shifted northward in both models by about 0.5° in latitude. The return flow of the Gulf Stream is weaker in both models. The Mann Eddy in both models is weaker than observed. The anti-cyclonic gyre around 51°N and 45°W in the Northwest Corner has similar strength with observations, but is overestimated in CREG12, and weaker in GBN36. The speeds of the Gulf Stream and North Atlantic Current in GBN36 are generally consistent with observations, but are larger in CREG12.

b. Root-mean square of sea level variability and eddy kinetic energy

Meso-scale eddy activity is assessed by analyzing SLA along satellite altimeter tracks and the surface geostrophic velocity normal to the tracks. The along-track altimeter data have a spatial resolution of 6.2 km which is considerably higher than that of gridded products (~30 km). The analysis of the mesoscale variability in the GBN area is based on 3-years of altimeter data and results from the two models.

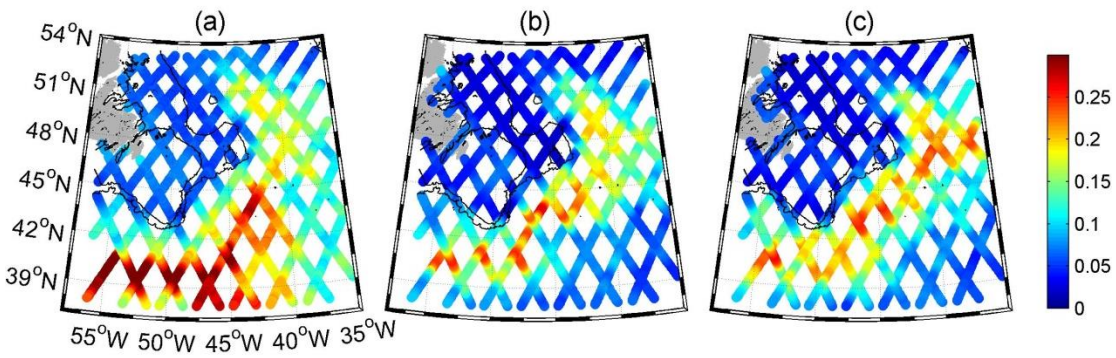

Figure 7: *Root mean square of SLA (in m) from (a) along-track altimeter data, (b) CREG12 and (c) GBN36. Data are unfiltered.*

Fig. 7 shows that the root-mean-squares (rms) of SLA from the altimeter data and the two models. Fig. 8 compares the EKE estimated from the surface geostrophic velocity normal to the altimeter tracks. The spatial distributions of these quantities show both agreement and disagreement. According to the altimeter data, the rms of SLA and EKE are high along the Gulf Stream and to the southeast of the Grand Banks with amplitudes greater than 20 cm and 1000 $cm^2\ s^{-2}$, respectively. Secondary maxima of rms and EKE are found to the north of Flemish Cap and the amplitudes are about 15 cm and 1000 $cm^2\ s^{-2}$. Low values of rms and EKE are found on the Labrador shelf and the Grand Banks with amplitudes of several centimeters and less than 200 $cm^2\ s^{-2}$, respectively. The two models show systematic differences with the altimeter data in the Gulf Stream and its downstream region. In both models, the eddy variability decreases too rapidly downstream of the Gulf Stream. The two models obtain much weaker rms of SLA and EKE over the Gulf Stream, although GBN36 obtains slightly higher EKE than CREG12. Both models obtain too weak eddy variability to the southeast of the NAC. To the east and north of Flemish Cap, CREG12 obtains similar rms of SLA and EKE as the altimeter data, while GBN36 overestimates this eddy variability.

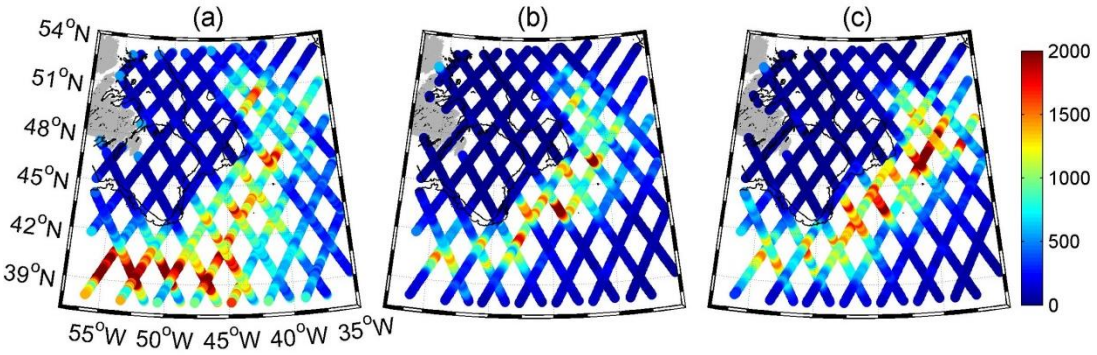

Figure 8: *Eddy kinetic energy of surface geostrophic currents (in $cm^2\ s^{-2}$) derived from (a) along-track altimeter data, (b) CREG12 and (c) GBN36. Low-pass filter with a cutoff at 30 km is applied to SLA from altimeter and models prior to computing geostrophic currents.*

c. Vertical structure of kinetic energy

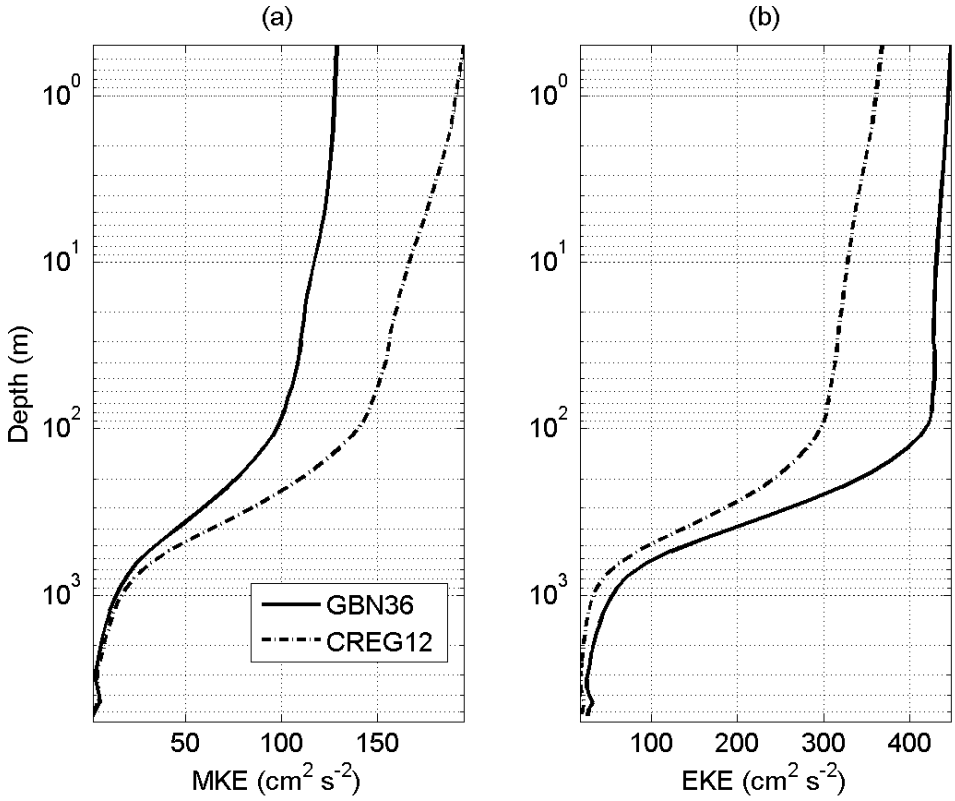

Figure 9: *Vertical profiles of (a) MKE and (b) EKE averaged over the study area for CREG12 (dashed curves) and GBN36 (solid curves).*

Figure 9 shows vertical profiles of MKE and EKE averaged over the study area for GBN36 and CREG12. Here MKE is computed from the time mean velocities, and EKE is computed from velocity deviations from time means. Both MKE and EKE display a three-layer structure: being nearly uniform from surface to 100 m depth, decreasing from 100 m to 1000 m, and weak at depths greater than 1000 m. The three-layered structure of EKE agrees with the box model solutions obtained by Böning and Budich (1992). The three-layered structure of MKE is consistent with the mean currents from instruments moored on the continental slope in the path of the Labrador Current (Petrie and Buckley, 1996), and snapshot profiles of the geostrophic flow across sections along the Gulf Stream and the North Atlantic Current (Clarke et al., 1980). Interestingly, in this study region as the model resolution increases from CREG12 to GBN36, the MKE decreases while EKE increases.

d. SLA spectra

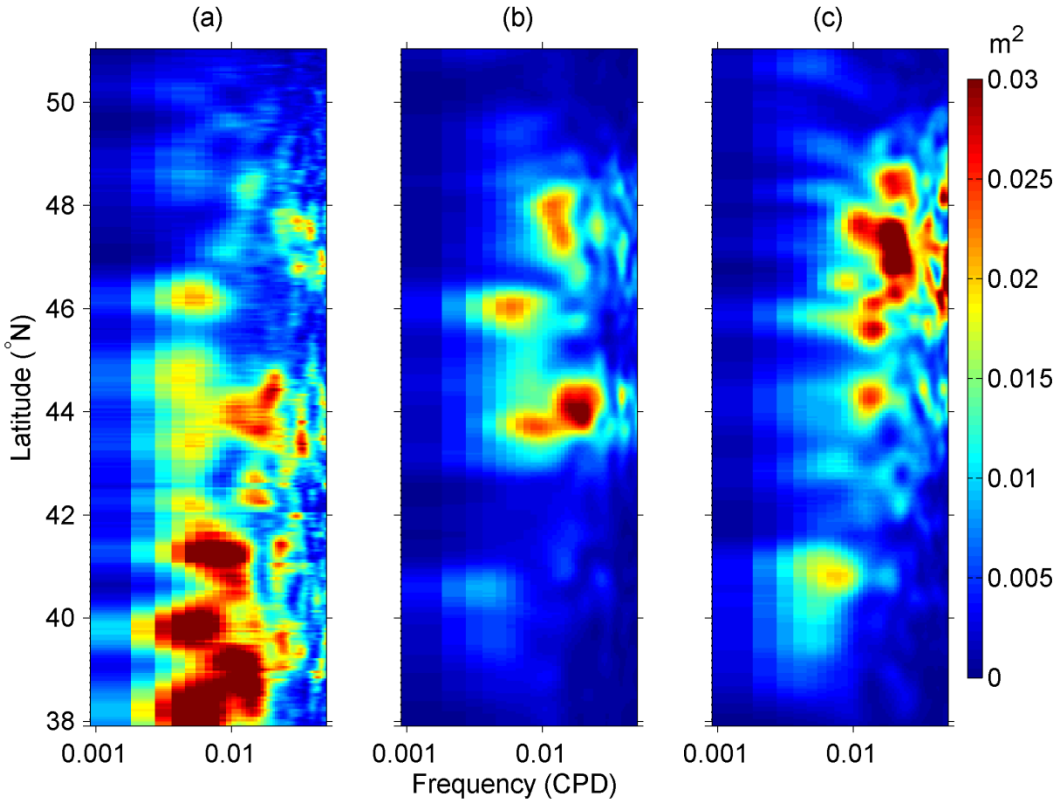

Figure 10: *Frequency spectra of SLA in variance-preserving form (in m^2) along the highlighted track marked in Figure 1, from (a) along-track altimeter data, (b) CREG12, and (c) GBN36. Data are unfiltered.*

The frequency and wavenumber spectra of SLA are computed for the SLA along a track over the path of the North Atlantic Current (track highlighted in Fig. 1). Figs. 10 and 11 show these spectra in variance-conserving form. Fig. 9 shows that spatial variability of the frequency spectra. In the southern part of the track (south of 43°N), the altimeter data shows high spectral energy but both models obtain very weak energy. Between 43°N and 46.5°N, CREG12 obtains two spectral peaks generally consistent with observations: one centered around 44° N and the 100-day period, and one centered around 46° N and the 200-day period. GBN36 obtains two peaks at similar locations but both with energy centered near the 100-day period. North of 46.5°N, CREG12 obtains similar level of spectral energy as the altimeter data, whereas GBN36 overestimates the spectral energy.

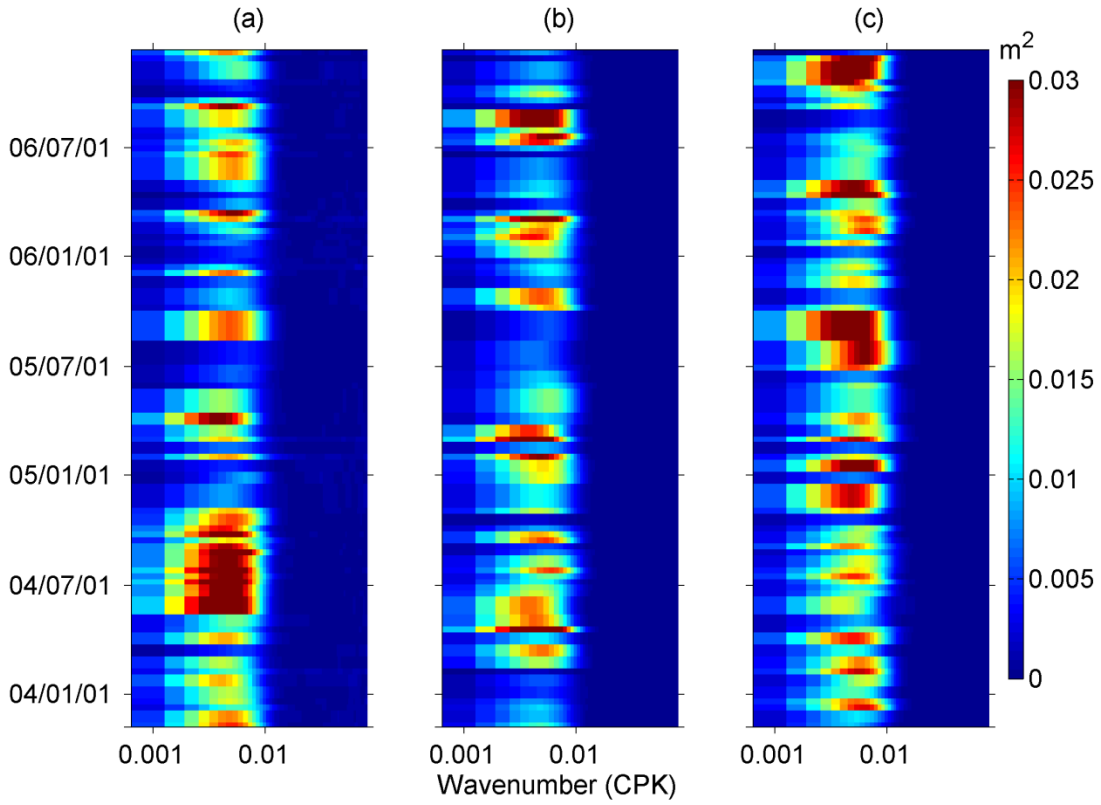

Figure 11: *Wavenumber spectra of SLA in variance-preserving form (in m2) from (a) along-track altimeter data, (b) CREG12, and (c) GBN36. The spectra are computed for the segment between 42.5 and 48.5°N along the highlighted track marked in Figure 1. Data are unfiltered.*

The wavenumber spectra of SLA are computed along the highlighted track in a segment bounded by 42.5°N and 48.5°N, where the rms of SLA and EKE are nearly uniform. Fig. 11 shows the time variations of the wavenumber spectra. Both modelled and observed spectra exhibit a similar energy-containing band at wavelengths between 100 km and 500 km. The mismatch between the observed and modelled spectra in time is expected because of the turbulent nature of eddy activity and no data assimilation being included in the models.

Due to the significant spatial variation of frequency spectra shown in Fig. 10, we scale the spectrum at each location by its total energy (variance of the SLA time series), and then average the scaled spectra from different locations. Fig. 12a shows the averaged spectra from the altimeter data and the two models. Despite the wide range of spatial variability of the spectra, the averaged spectra from the two models are close to observations at all periods (Fig.12a). Similarly, each wavenumber spectrum shown in Fig. 11 is scaled by its total energy, and then the scaled spectra from different time periods are averaged. The resulting averaged spectra are shown in Fig. 12b. The range of temporal variation of the scaled wavenumber spectra is much narrower than that of spatial variation of the scaled frequency spectra. The averaged wavenumber spectra from the two models show close agreement with the observed one. At the higher wavenumber end, the observed spectrum shows elevated energy compared with modelled spectra due to noise contained in the altimeter data.

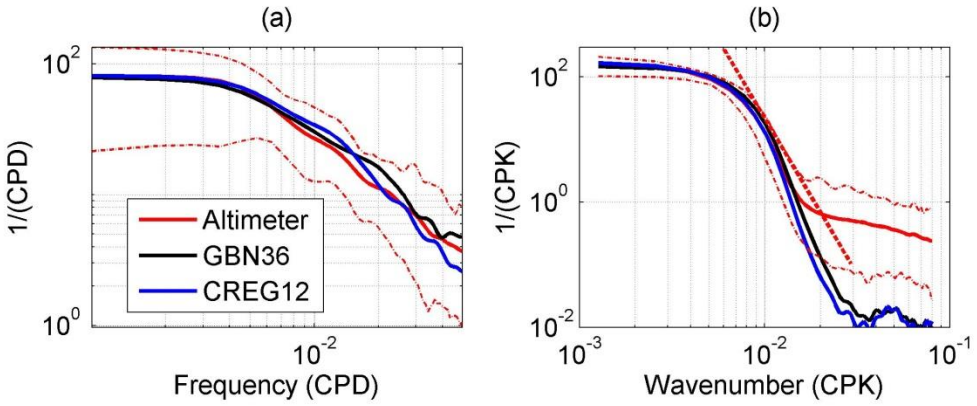

Figure 12: *(a) The spatial average of frequency spectra of SLA (shown in Fig. 10) after each spectrum is scaled by its total energy (variance of the time series), and (b) the temporal average of wavenumber spectra of SLA (shown in Fig. 10) after each spectrum is scaled by its total energy (variance of the along-*

track SLA) Dash-dotted curves denote 95- and 5-percentiles of observed spectra. The dashed straight line in (b) denotes slope of p=-5.

The wavenumber spectra of SLA closely follow a slope of -5 on logarithmic power spectral density scales at the wavelength of around 100 km. Two wavenumber regimes of SLA may be described as: an energy containing band with a very flat spectrum at wavelength > 100 km, and a steep decay of energy close to p=-5 at wavelength < 100 km. The interpretation of the wavenumber spectrum slope is closely related to theories of two-dimensional (2D) geostrophic turbulence generated by baroclinic instability (Kundu and Cohen, 2004; Olbers et al., 2012). The spectral slope of p=-5 along this particular track is consistent with the slope previously discovered near strong currents (Fu, 1983).

e. Summary

At the first stage of GBN36 development, we evaluate model performance with MDT, drifter and along-track SLA data. Both MDT and drifter data have coarser spatial resolution than the models. The along-track altimeter data provide estimates of SLA and surface geostrophic currents. Additional data from in situ observations, such as ADCP/LADCP, tide gauge and CTD data, are needed to evaluate model solutions at depth. In turn the model results can help to interpret the discrete in situ measurements. Clearly, the results of this study are preliminary. Further tests of model parameterization, input data, and evaluation with more observational data are needed to obtain a more quantitative description of the ocean currents and eddy variability in this region.

Part 2: A 3-year (2013-2015) hindcast with GBN36 based on NEMO v3.6

For this task, GBN36 takes initial and lateral boundary condition from the PSY4 operational global analysis from Mercator-Ocean, France. The surface atmospheric forcing is the hourly field from the blending of the global deterministic prediction system (DPS) and the regional DPS, with horizontal resolutions of 30 km and 10 km respectively, from the Canadian Meteorological Centre. A 3-year hindcast covering 2013-2015 is carried out. In this analysis, we define anomalies as variables with monthly means removed. Here we provide a summary of key results.

a. Sea levels

Hourly water levels at tide gauge stations (Fig. 13) are adjusted for the inverse barometer (IB) response using hourly sea level pressure (SLP) data of Climate Forecast System Version 2 (CFSV2, Saha et al., 2014). The IB-adjusted water levels are 48-hour low-pass filtered, and 2-day averaged. Modelled sea levels are extracted onto the latitudinal and longitudinal locations of tide gauges.

Figure 14 compares monthly mean sea levels. GBN36 and PSY4 show consistent seasonal variability with observed water levels. The maximum sea levels occurred in November or December, and minimum in May or June. Both models slightly underestimate the magnitude of seasonal cycle.

Figure 15 compares the standard deviations (std) of sea level anomalies, with greater values in winter, possibly resulted from stronger wind. GBN36 and PSY4 show similar variability with observations, however, slight underestimation of magnitude, in particularly in winter in St John's and Bonavista stations.

Figure 16 shows that GBN36 and PSY4 obtain similar spectra, however, significantly weaker variability at periods greater than 5 days and most significantly at periods greater than 10 days. This is possibly due to weaker shelf-trapped waves as both models do not include air-pressure forcing.

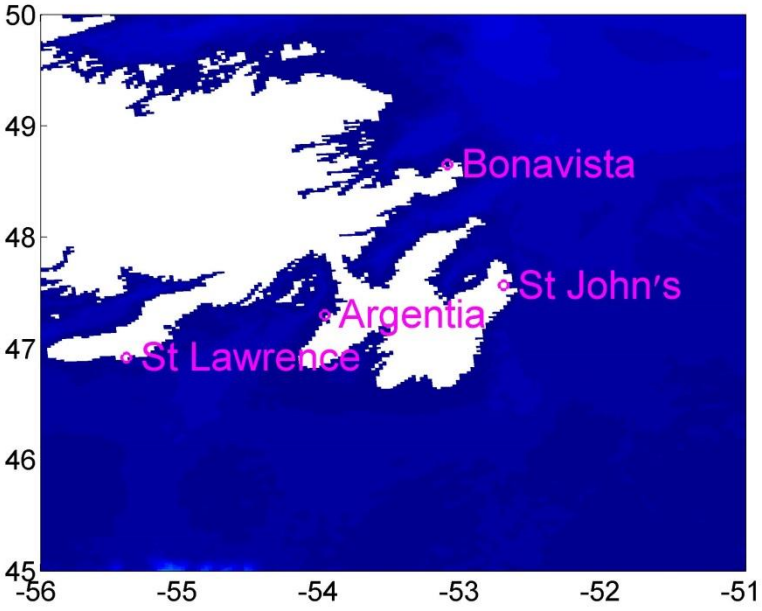

Figure 13: *Tide gauge stations in Newfoundland.*

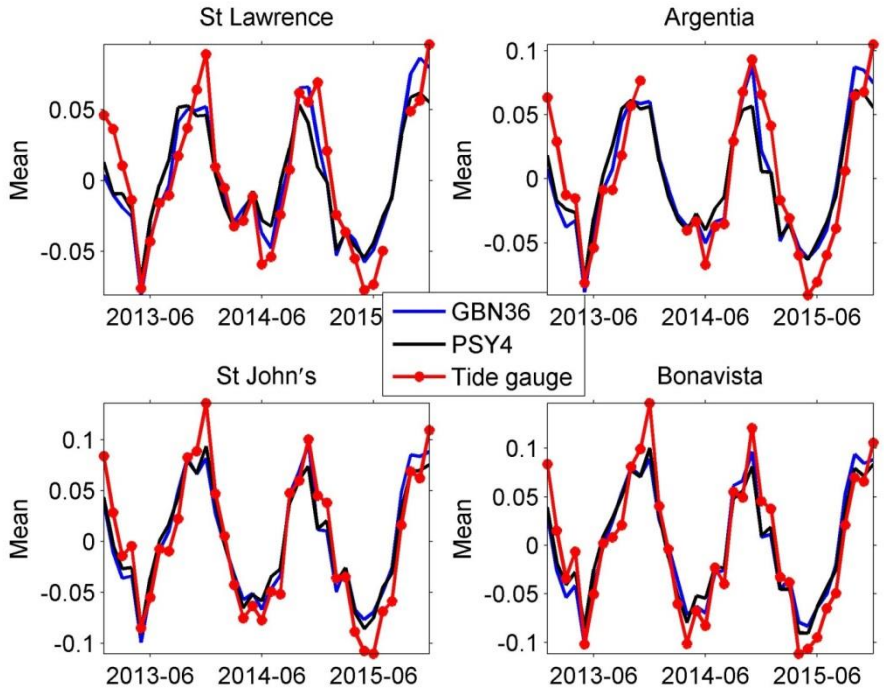

Figure 14: *Monthly means of sea levels modelled by GBN36 (blue) and PSY4 (black), compared to monthly means of observed sea levels with inverse barometric response removed (red).*

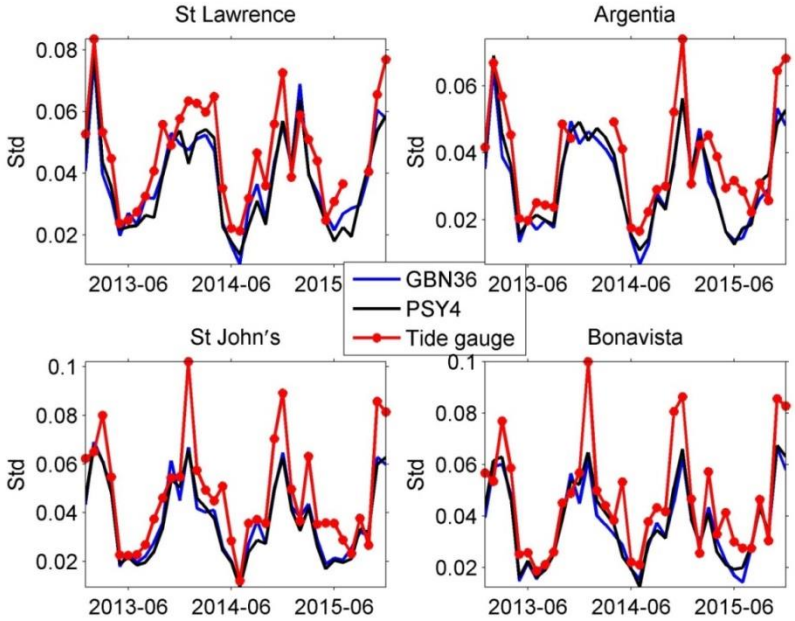

Figure 15: *Standard deviations of sea level anomalies modelled by GBN36 (blue) and PSY4 (black), compared to standard deviations of observed sea level anomalies with inverse barometric response removed (red).*

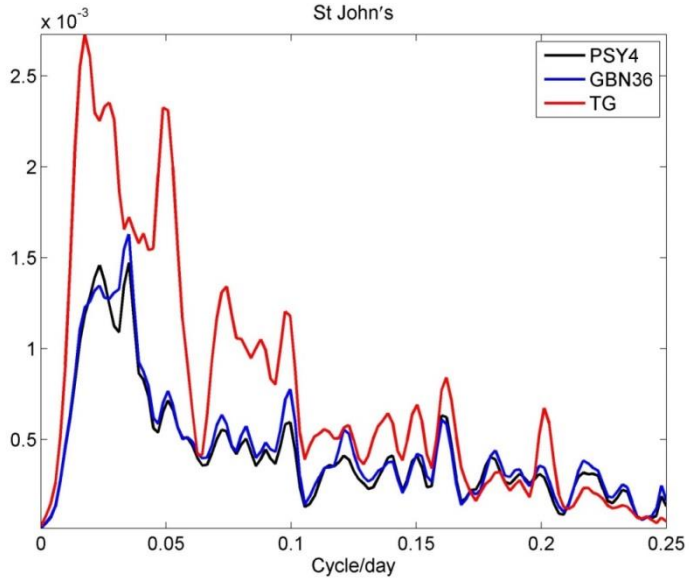

Figure 16: *Variance conserving spectra of sea level anomalies modelled by GBN36 (blue) and PSY4 (black), compared to variance conserving spectra of observed sea level anomalies with inverse barometric response removed (red).*

b. Sea Surface Temperature

Sea surface temperature (SST) obtained from OSTIA analysis is used to evaluate modelled SST. OSTIA (http://ghrsst-pp.metoffice.com/pages/latest_analysis/ostia.html) uses satellite and in situ observations to determine SST. The analysis is produced daily at a resolution of 5 km.

Figure 17 shows the bias in each season, calculated as the model estimate minus the observation. The warm bias is most significant (1-5 °C) in deep water around Grand Banks, and is about 1 °C on the Newfoundland Shelf. Cold biases are in isolated spots in deep water. On the Grand Banks, the biases are insignificant.

Figure 18 shows standard deviations of OSTIA SST anomalies for 4 seasons. On the shelf, variability is lowest in winter, and is about 1-1.5°C in other seasons. In deep water, significant variability is around Grand Banks, lowest in summer (~1°C) and strong in spring & fall (1.5-2°C).

Figure 19 shows standard deviations of GBN36 SST anomalies in each season. On the Shelf, again the lowest variability is in winter. In deep water around Grand Banks, again lowest variability is in summer. But GBN36 & PSY4 both show stronger variability than OSTIA in eddy-rich areas, possibly due to smoothing in OSTIA.

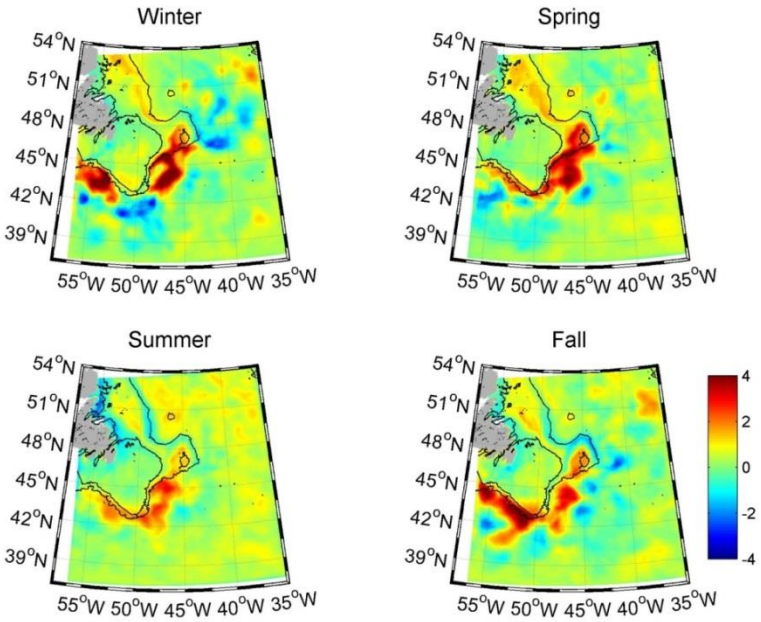

Figure 17: *Seasonal means of GBN36 minus OSTIA SST.*

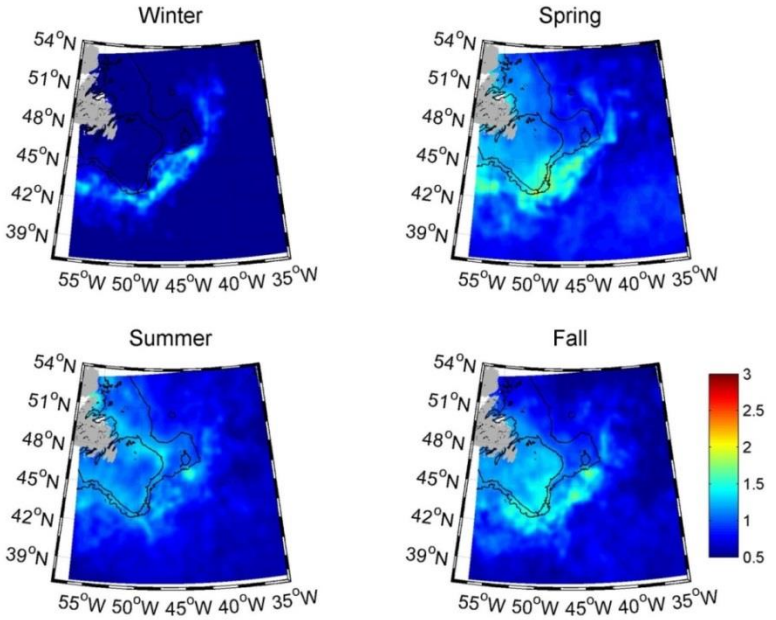

Figure 18: *Standard deviations of OSTIA SST anomalies for 4 seasons.*

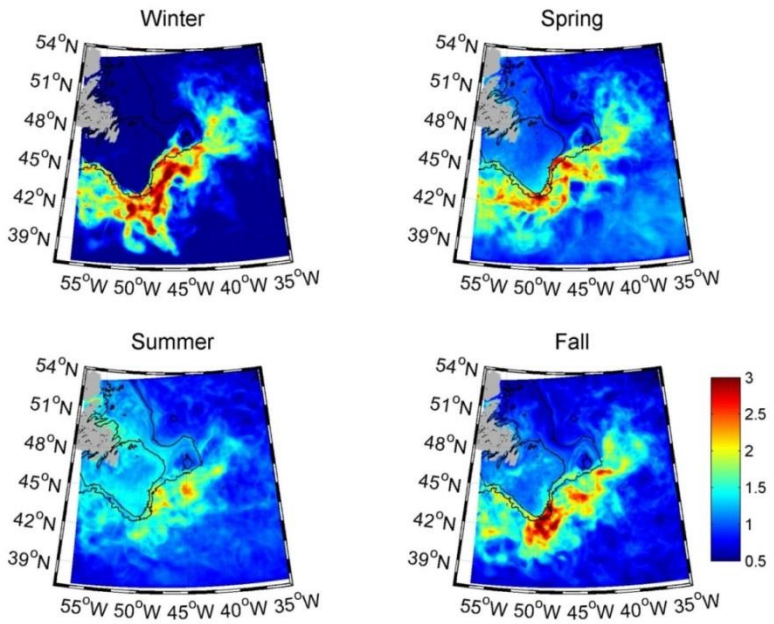

Figure 19: *Standard deviations of GBN36 SST for 4 seasons.*

c. Water Column Temperature and salinity

Measurements of temperature and salinity profiles are obtained from the Atlantic Zone Monitoring Program (AZMP). Model values are extracted at the same time and locations as observations.

The profiles on the Grand Banks (Figure 8) show GBN36 and PSY4 simulate well the vertical structure of temperature and salinity. Both models reproduce the feature of cold intermediate water. There is a salty bias (< 0.6 psu) in both models in top 300 m. Standard deviations of T/S show a S-shape decrease with depth in top 500 m.

The profiles in deep water south of the Grand Banks modelled by GBN36 and PSY4 agree with CTD observations (Figure 20). There is a salinity maxima of centered around 200 m depth. Most variability of T/S is above 1000 m, and standard deviations decrease with depth.

d. Currents

LADCP measurements at 47°N between 44° and 36° W were carried out on six different cruises between 2003 and 2011 (Mertens et al., 2014). These are compared to 3-year mean of modelled velocities in Figure 21. Measured circulation along a zonal section at 47 ^{o}N shows a deep reaching North Atlantic Current (NAC) with adjacent recirculation and two distinct cores of southward flow in the Deep Western Boundary Current (DWBC). This structure is well reproduced in the GBN36 model using the Smagorinsky scheme and PSY4 model. GBN36 model using $A_M = 10^8$ m^4 s^{-1} produces weaker flows than observations.

e. Summary

At this stage of GBN36 development, we evaluate model performance with tide gauge, SST analysis, CTD and LADCP data. In general, GBN36 does good job in simulating sea levels, SST, T/S vertical structures and mean transports.

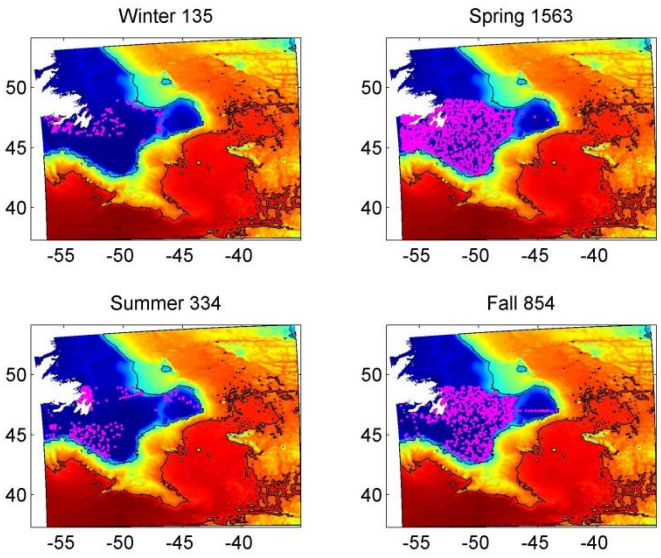

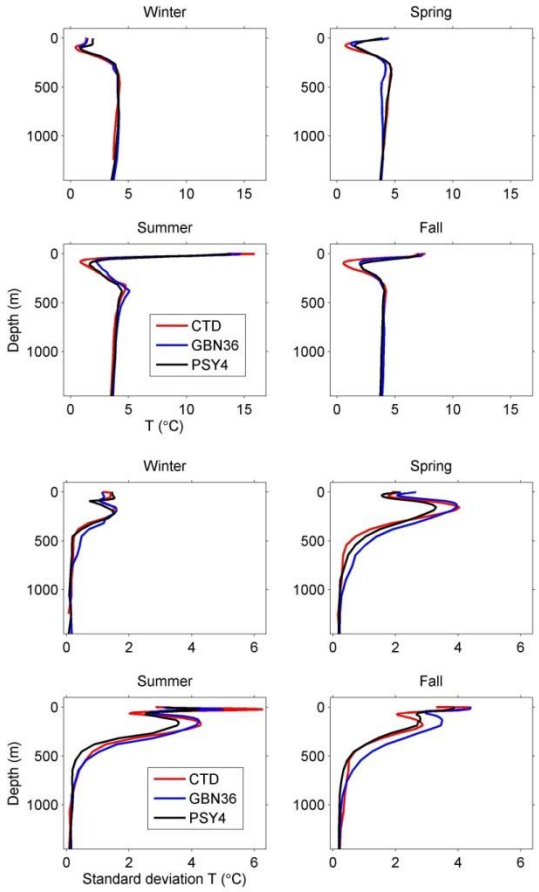
Winter
Spring
Summer
Fall
Depth (m)
CTD
GBN36
PSY4
T (°C)
Winter
Spring
Summer
Fall
Depth (m)
CTD
GBN36
PSY4
Standard deviation T (°C)

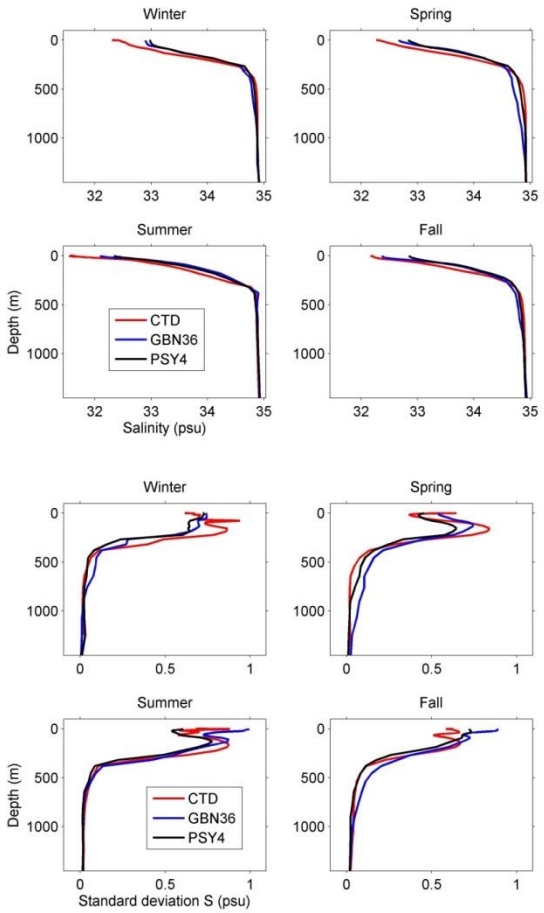

Figure 20: *(Top) CTD stations on the Grand Banks of Newfoundland. (Middle left) vertical profiles of average temperature and (Middle right) standard deviations. (Bottom left) vertical profiles of average salinity and (Bottom right) standard deviations.*

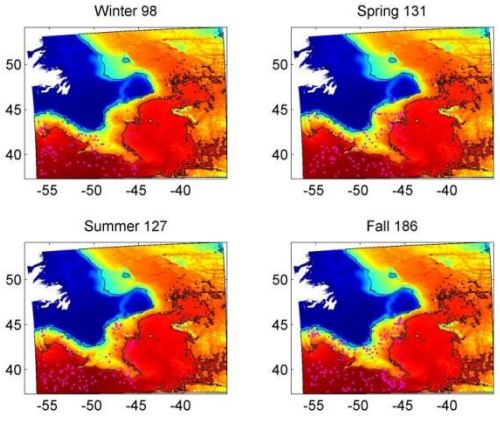

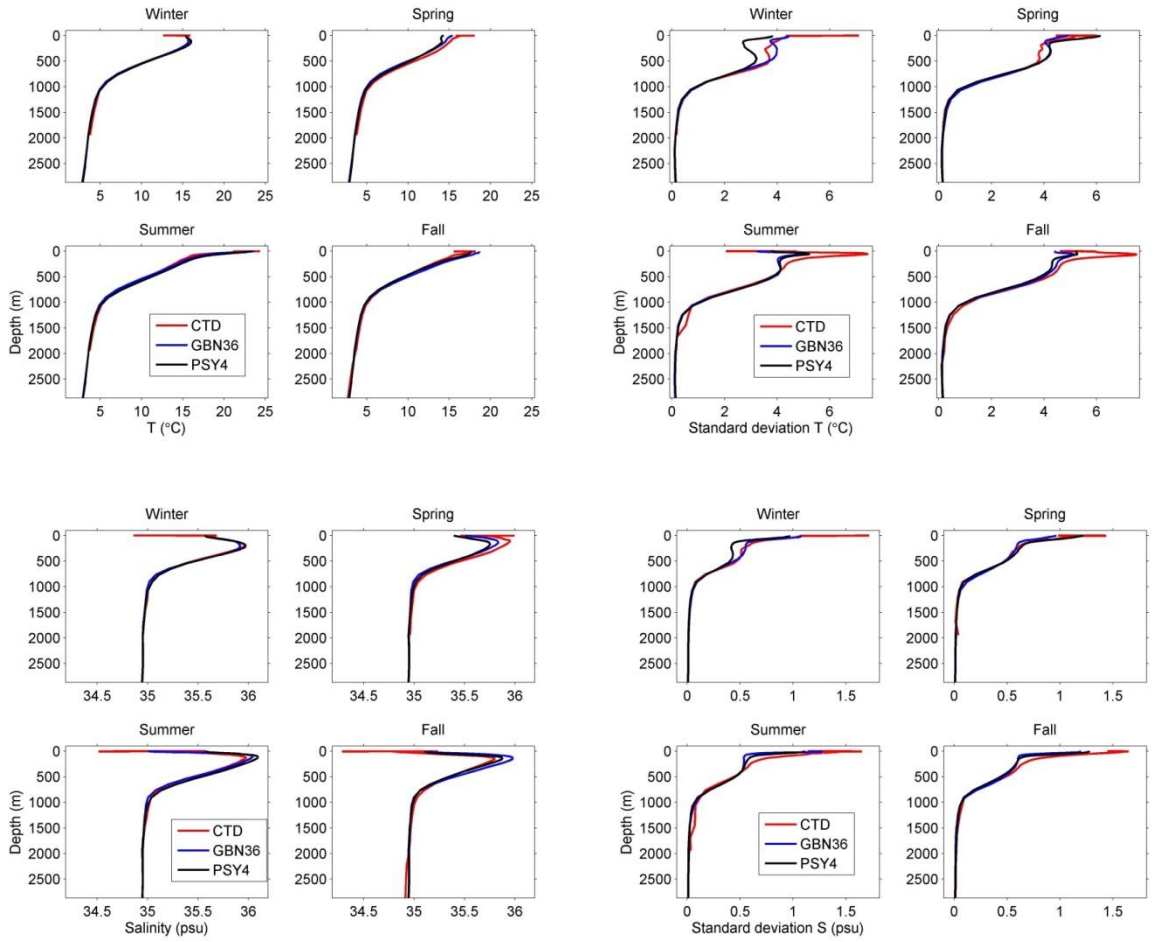

Figure 21: *(Top) CTD stations in deep water south of the Grand Banks. (Middle left) vertical profiles of average temperature and (Middle right) standard deviations. (Bottom left) vertical profiles of average salinity and (Bottom right) standard deviations.*

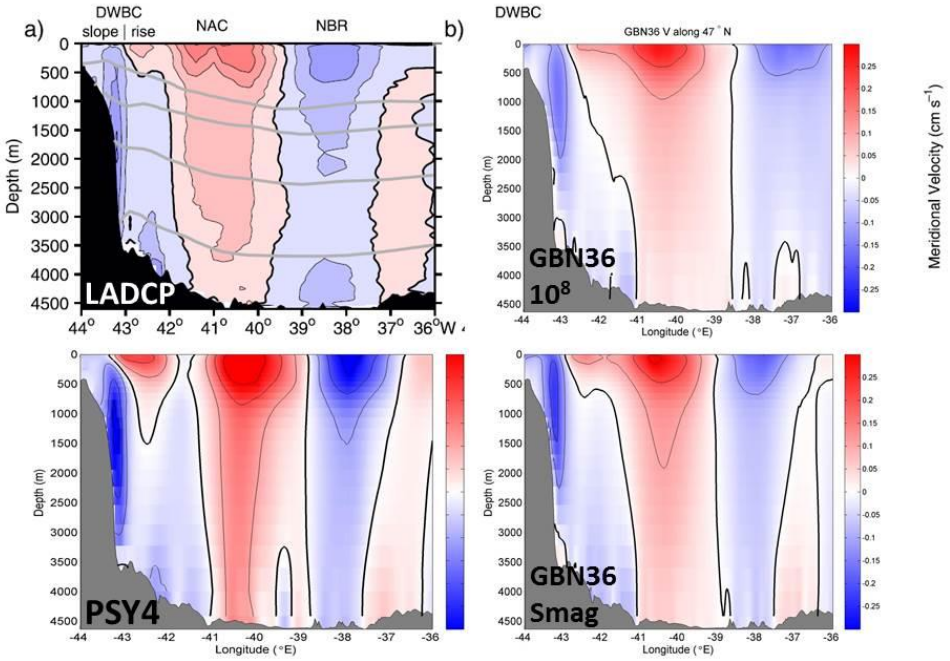

Figure 21: *a) Mean meridional velocity along 47°N from LADCP measurements carried out on six different cruises (Mertens et al., 2014). 3 year mean of meridional velocity along 47°N from b) GBN36 model using $A_M = 10^8$ m^4 s^{-1}, c) PSY4 model and d) GBN36 model using the Smagorinsky scheme.*

Annex B

Task 2: Technical Report Improved Ocean Analysis

Introduction

In order to provide a skillful forecast, it is essential that an accurate estimate of the current ocean conditions are available to initialize the ocean model. Given the relatively slow timescales of the ocean as compared to the atmosphere, the skill of an ocean forecast will depend highly on the quality of the initial condition. This is in contrast to atmospheric weather forecasts, where the weather systems evolve on the timescales of the forecast lead time (e.g. 3-5 days) and thus the model plays roughly an equivalent role to the analysis in terms of affecting forecast error.

Two approaches to produce ocean state estimates are used in this project. The first, involves integrating all available ocean observations with a numerical estimate of the ocean state using a least-squares fit based on the relative error of the model and observations; a process referred to as “data assimilation”. This approach follows closely what is used in numerical weather prediction. A second approach is used to generate high resolution (kilometer scale) initial conditions where sufficient observations are not available to adequately constrain the small scales. For this, the high-resolution model is pushed towards the lower resolution analyses produced using data assimilation, in such a way that allows the small scales to remain. These small scales are generated by the model based on the representation of the coastal processes (e.g. due to bathymetry and tides). In this way the large-scale ocean state can be “downscaled” to include the details from the coastal ocean model.

In this section, the work to improve both these aspects is presented. First, the improvements to the SAM2 data assimilation system used in the GIOPS system is presented. These improvements have now been incorporated in the operational system running at CCMEP called GIOPSv2.1. Second, the spectral nudging approach developed to initialize the high resolution system for the Grand Banks is presented.

Improved Data Assimilation Methods in GIOPS

SAM2 is a data assimilation tool designed for the regional and global oceans which has been developed with different NEMO configurations by Mercator-Océan. A detailed description of SAM2 can be found in the GIOPSv1.1 Technical Documentation.

Observations Assimilated

SAM2 assimilates three types of observations: direct scalars (DS; e.g. sea surface temperature), indirect scalars (IS, e.g. sea level anomaly) and vertical profiles (VP; e.g. Argo). In GIOPSv2.1 bogus observations (observations with innovation set to zero) are also employed.

DS observations in GIOPSv1.1 consist of the CCMEP gridded SST analysis product at 0.2° resolution and pseudo observations of the barotropic height (Hbar). The latter are no longer used in GIOPSv2.1. SST observation measurement error in GIOPSv2.1 has been reduced from 0.3°C to 0.2°C. This change was made to reduce differences between the analysis and the CCMEP SST that are larger in GIOPSv2.1 due to use of an Incremental Analysis Updating (IAU) procedure (described below).

The IS observations are taken from the SSALTO/DUACS AVISO Near-Real Time Along-Track product as for GIOPSv2.1. As the observations have been filtered to remove effects such as tides, and inverse barometer (due to variations in atmospheric pressure), a similar filtering is applied to the model SSH as part of the observation operator. At the time of writing, three satellite altimeters were being used: Jason2, Cryosat2 and Saral/Altika. Observation measurement errors for all three instruments are set to 2 cm as was used for GIOPSv1.1. One of the main changes introduced in GIOSPv2.1 is the use of an improved mean dynamic topography (MDT) field and associated error field.

The MDT used to assimilate SLA observations is very important as it affects the constraint on the mean circulation of the model, such as the Gulf Stream, the Kuroshio Current, the North Atlantic Current. GIOPSv1.1 used an objective analysis mapping of the MDT from altimetry, hydrology, drifters and gravimetry (Rio and Hernandez, 2004). GIOPSv2.1 uses a more recent MDT derived from the CLS-CNES09 product produced using Argo profile data and improved

gravimetry from the GOCE satellite mission (Rio et al. 2011). The MDT used in GIOPSv2.1 includes modifications to CLS-CNES09 using mean innovations from the GLORYS reanalysis (Lellouche et al., 2009). The two MDT fields are shown in Fig. 22.

VP observations are obtained from Collecte Localisation Spatiale, as is done by Mercator-Océan. No change to this dataset has been made in GIOPSv2.1. Additional information regarding the in situ data types, volumes and transmission delays are available in the GIOPSv1.1 Technical Documentation.

The use of bogus observations has been introduced in GIOPSv2.1. These "observations" are composed simply of a location, time and error for which an innovation of zero is assigned. This allows the assimilation system to be constrained toward its background field in certain areas. In GIOPSv2.1 bogus observations have been applied to temperature and salinity in three areas: in the vicinity of large river mouths to avoid the assimilation of low salinity values; in the subsurface equatorial pacific to reduce negative effects on the equatorial undercurrent from assimilation of SLA observations; and under sea ice to avoid contamination from spurious covariances due to the SST assimilation and imbalances introduced by the sea ice assimilation.

Assimilation Method

GIOPSv2.1 uses a significantly updated version of the SAM2 code. Modifications to the code include technical changes to make the code more efficient and portable, and notably, to remove a dependence on the PALM sequencer. A number of new features have been added to the code as well. In particular, the use of an Incremental Analysis Updating (IAU) approach has been introduced to avoid shocks when adding increments. A schematic of the scheme is shown in Fig. 23. In GIOPSv2.1, the IAU scheme has been configured to apply the analysis increments evenly over the last day of the cycle (day 7 for the GR weekly and the full cycle for GU daily). This requires re-running the model over the last day. Note that due to non-linearities in the model, the new "analysis" obtained at the end of the IAU run, will not be exactly equal to the sum of the trial field and the increment (as was the case for GIOPSv1.1). This scheme significantly reduces gravity wave noise in the system, as permits a smoother and more physical

evolution of model fields. An example of the impact of the IAU scheme on equatorial instability waves in the Equatorial Pacific Ocean is shown in Fig. 24.

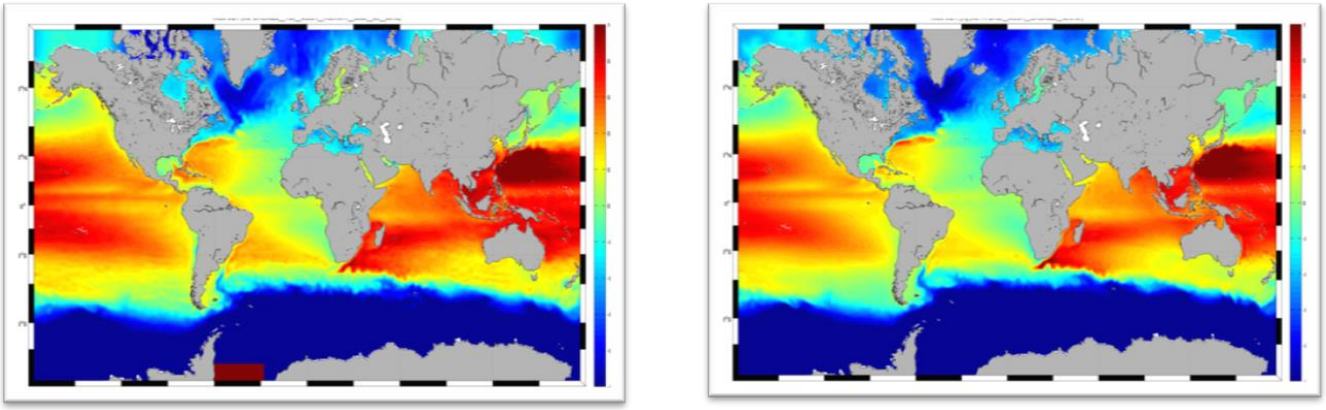

Figure 22: *Mean dynamic topography used in GIOPSv1.1 (left) and GIOPSv2.1 (right). Note the significant increase in sea level gradients across the Gulf Stream.*

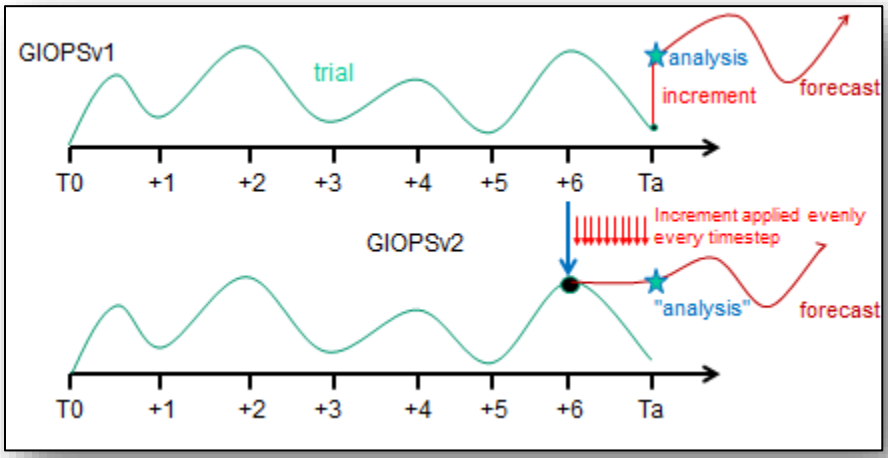

Figure 23: *Schematic of the Incremental Analysis Updating (IAU) procedure. Analysis increments are applied evenly over the last day of the cycle (day 7 for the weekly cycles).*

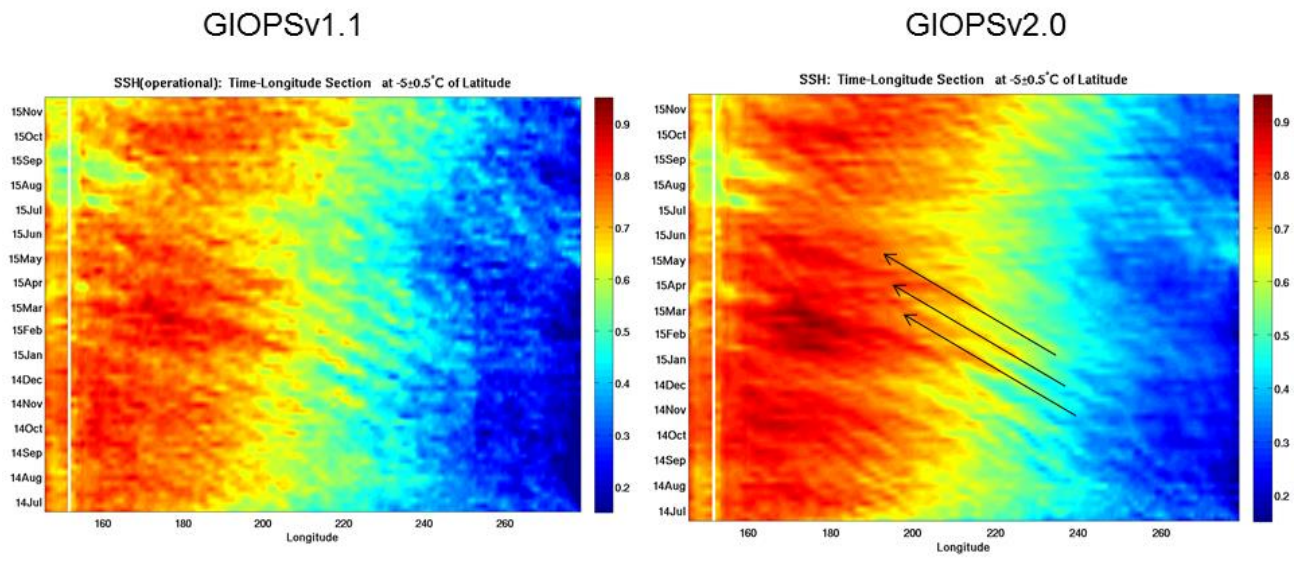

Figure 24: *Evolution of sea surface height fields in the Equatorial Pacific Ocean. Meridionally-averaged SSH fields from 5°N to 5°S are shown for the period July 2014 to November 2015 for GIOPSv1.1 (left) and GIOPSv2.1 (right). Note the reduction in small scale noise and smoother propagation of Equatorial Instability Waves to the west in GIOPSv2.1 (indicated with arrows).*

Implementation details

In order to provide the best quality daily analysis given the inherent delays in the observation system, GIOPS has been implemented using a 3-tier approach (Figure 25). The backbone of the system which provides the continuity in time is provided by the weekly delayed model analysis (GD) produced each week on Tuesdays, valid for the previous Wednesday at 00Z. The GD analysis is used to initialize the real-time weekly analysis (GR), produced on Wednesdays and valid that day at 00Z. In GIOPSv1.1, a GR daily update was run from Thursday to Tuesday to provide a daily analysis. The GR weekly and GR daily analyses were available at around 0400 UTC. To reduce the delay in availability of GIOPS analyses, GIOPSv2.1 produces daily analyses every day of the week (including Wednesday), providing analyses by 0100 UTC. The system nomenclature was changed to reflect this modification, with the daily analysis now being called GU. To make this change possible the dependency on the GDPS (G1) 00Z forecast for the GIOPS analysis validity date had to be removed. This was done by changing the source of atmospheric

forcing for GIOPS to use hours 12-33 of successive GDPS (G1) 12Z forecasts (instead of hours 6-27 of successive 00Z forecasts). The 6 hr increase in forecast lead time could be expected to result in slightly larger errors in atmospheric forcing fields and thus degraded GIOPS analysis quality. A full-year GD cycle was run with and without the change in forcing and no discernible impact on analysis quality was found.

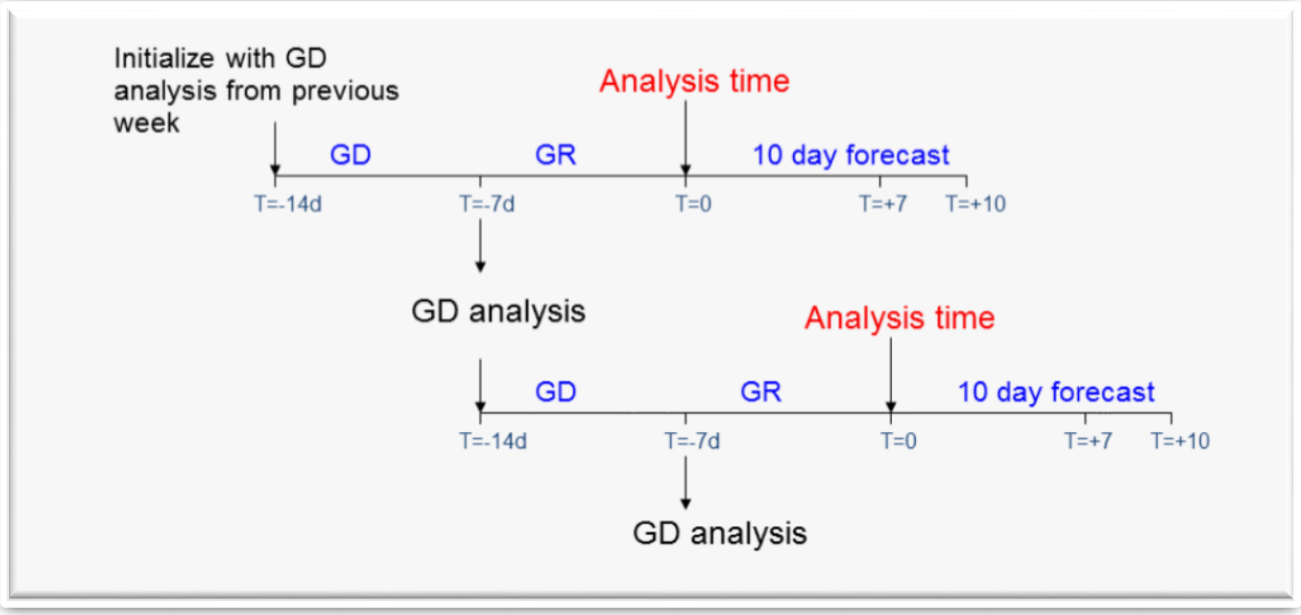

Figure 25: *Schematic showing the functioning of the GIOPS delayed (GD) and real-time (GR) analyses. All analyses are valid at 00Z. The GD is produced on Tuesdays and the GR on Wednesdays. GU analyses for other days are produced using 1-day assimilation window and assimilating SST only.*

Blending of ice and ocean analyses

Prior to model initialization (i.e. for either a trial or a forecast), the SAM2 ocean analysis is blended with the operation 3DVar sea ice analysis. Details of the blending method have not been changed from GIOPSv1.1 and can be found in Smith et al. (2015). However, two small technical changes to the sea ice blending have been made. First, to improve consistency with the GIOPS forecast suite and reduce the delay in availability of GIOPS analyses, the 18 UTC ice analysis for the previous day is used (instead of the 00 UTC analysis). This change did not impact

the analysis quality significantly as 18 UTC analyses are the only ice analysis that include daily ice charts from the Canadian Ice Service. The other analyses (00 UTC, 06UTC and 12 UTC) assimilate only passive microwave satellite observations. Additionally, the blending is now made at the end of the analysis suite rather than at the beginning of the subsequent suite (either analysis or forecast) as was done in GIOPSv1.1.

Verification methods

Evaluation of GIOPS analyses is made following the method outlined in the GIOPSv1.1 Technical Documentation. In brief, mean and root-mean-squared (RMS) innovation statistics automatically generated by SAM2 over 46 pre-defined regions for all assimilated data types (altimetry, SST, in situ) are assessed. The 46 regions used were defined by Mercator and are left unchanged to allow for a direct comparison with the Mercator systems. A map showing the location of these regions is provided in Figure 26 and the names of the regions is provided in Table I. Not that the regions do not cover all areas of the ocean, but rather were chosen to isolate particular physical processes. Additionally, GIOPS SST analyses are compared to operational CCMEP SST analyses in terms of spatial maps of mean and RMS differences.

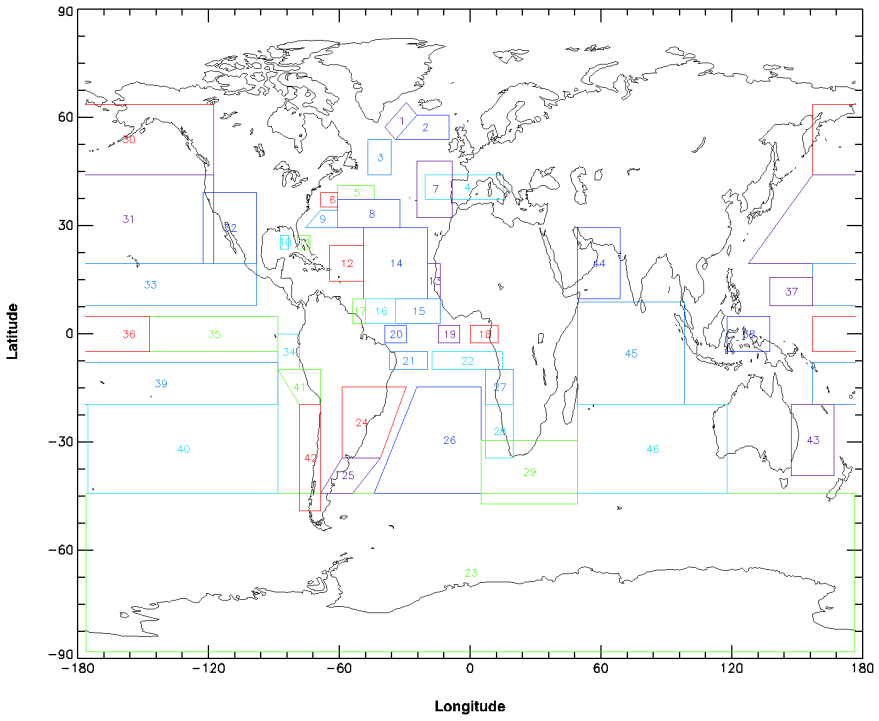

Figure 26: *Global map showing the 46 pre-defined regions used by GIOPS to evaluate innovation statistics.*

Table 1: *Names of the 46 pre-defined regions used to evaluate innovation statistics.*

0	Global	23	Antarctic_Circumpolar_Current
1	Irminger_Sea	24	South_Atlantic
2	Iceland_Basin	25	Falkland_current
3	Newfoundland-Iceland	26	South_Atl._gyre
4	Yoyo_Pomme	27	Angola
5	Gulf_Stream2	28	Benguela_current
6	Gulf_Stream1_XBT	29	Aghulas_region
7	North_Medeira_XBT	30	Pacific_Region
8	Charleston_tide	31	North_Pacific_gyre
9	Bermuda_tide	32	California_current
10	Gulf_of_Mexico	33	North_Tropical_Pacific
11	Florida_Straits_XBT	34	Nino1+2
12	Puerto_Rico_XBT	35	Nino3
13	Dakar	36	Nino4
14	Cape_Verde_XBT	37	Nino6
15	Rio-La_Coruna_Woce	38	Nino5

16	Belem_XBT	39	South_tropical_Pacific
17	Cayenne_tide	40	South_Pacific_Gyre
18	Sao_Tome_tide	41	Peru_coast
19	XBT_-_central_SEC	42	Chile_coast
20	Pirata	43	Eastern_Australia
21	Rio-La_Coruna	44	Indian_Ocean
22	Ascension_tide	45	Tropical_indian_ocean
		46	South_indian_ocean

As the primary applications of GIOPS are associated with surface features (sea ice, SST, surface currents) the focus of forecast verification is also in terms of surface features, and in particular, the SST and sea ice. Verification scores are produced using model forecasts as a function of lead time (for each forecast day) and the persistence of GIOPS and CCMEP SST analyses. Do to the smaller scales present in the GIOPS fields with respect to the CCMEP SST analyses, a Shapiro filter is applied (21 passes corresponding to roughly 1° resolution). Mean and RMS errors are evaluated both as spatial maps as well as a function of lead time over the various sub-regions of the global oceans (as shown in figure 27)

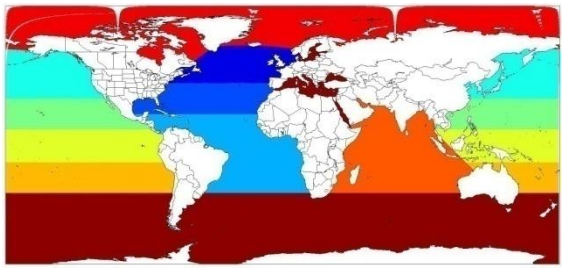

Figure 27: *Sub-regions of the global oceans used for SST forecast verification. The regions are: Subpolar North Atlantic (dark blue), Subtropical North Atlantic (medium blue), Equatorial and South Atlantic (light blue), North Pacific (cyan), Subtropical North Pacific (green), Equatorial Pacific (yellow), Subtropical South Pacific (orange), Indian (dark orange), Arctic (red), Southern Ocean (deep red).*

Sea ice forecasts are evaluated primarily using the two methods developed for the Regional Ice Prediction System (RIPS): comparison against ice analyses using the analysis tendency method, and dichotomous verification using the binary IMS analyses. For a detailed description of the methods please consult the RIPS technical documentation.

Evaluation of innovations

Here we present a comparison between the innovation statistics from the two versions of GIOPS for the period 2014-07-01 to 2015-09-01. The intent is to demonstrate the global and regional analysis skill and highlight areas of relative improvement and reduced skill. The scores presented represent spatial means calculated over the 46 predefined regions shown in Figure 26 and described in Table 1. Region 0 covers the entire global domain.

Overall, the innovations statistics show a significant improvement in GIOPSv2.1. In particular, a reduction of SLA error is found in most regions, with near-neutral scores for SST and in situ temperature and salinity.

Sea level anomaly (SLA)

The timeseries of global mean SLA innovations and RMS differences are shown in Figure 28 for Saral/Altika. Results obtained for the other two altimetry products (Jason2 and Cryosat2) are equivalent. Remarkably, GIOPSv2.1 shows important reductions in both bias and RMS errors, with a 17% reduction in the latter. The global mean RMS errors over the evaluation period for GIOPSv2.1 and GIOPSv1.1 are 6.90 cm and 8.23 cm respectively. This improvement is due mainly to the improvement in MDT (about 1cm reduction in RMS) with the rest due to a combination of factors (IAU, improved adaptivity scheme, modification to 21-day mean SLA field used in observation operator). Reductions in RMS error are found in almost all regions in both the Northern (Figure 29) and Southern (Figure 30) Hemispheres. The only regions showing slight increases in error are Nino4 and Nino5. These increases appear to be related to a mismatch in SSH imposed by the MDT. While many regions show a constant offset in SLA RMS error, some regions show a distinct improvement in the stability of the system related to the use of the IAU (Figure 31). In particular, in the central and eastern equatorial Pacific and Equatorial Indian Ocean small and more stable error statistics are obtained. In these regions, GIOPSv1.1 shows highly variable RMS error statistics due to the generation of spurious gravity wave noise excited by the addition of the analysis increment. Use of the IAU in GIOPSv2.1 is successful in reducing this error considerably.

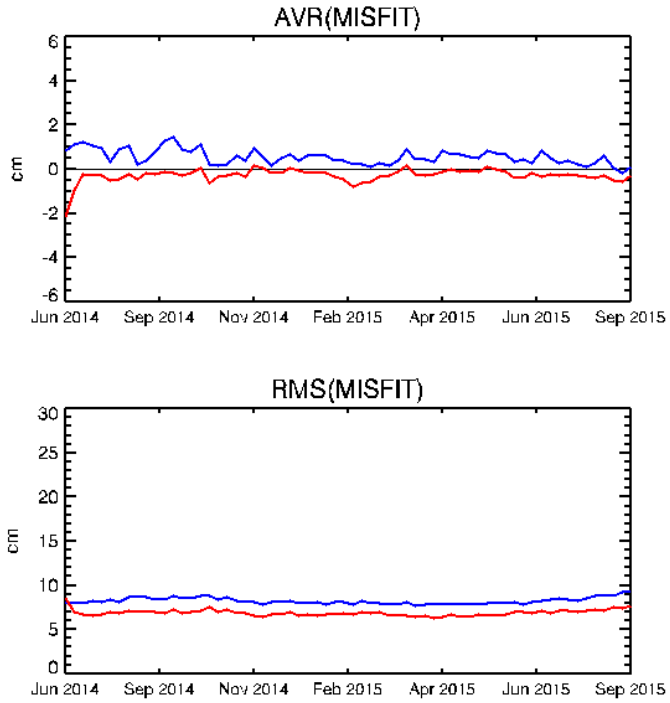

Figure 28: *Timeseries of global mean SLA innovations for GIOPSv2.1 (red) and GIOPSv1.1 (blue). The mean (top row) and root-mean-squared (RMS) differences (bottom row) are shown for both systems. Statistics are shown for Saral/Altika.*

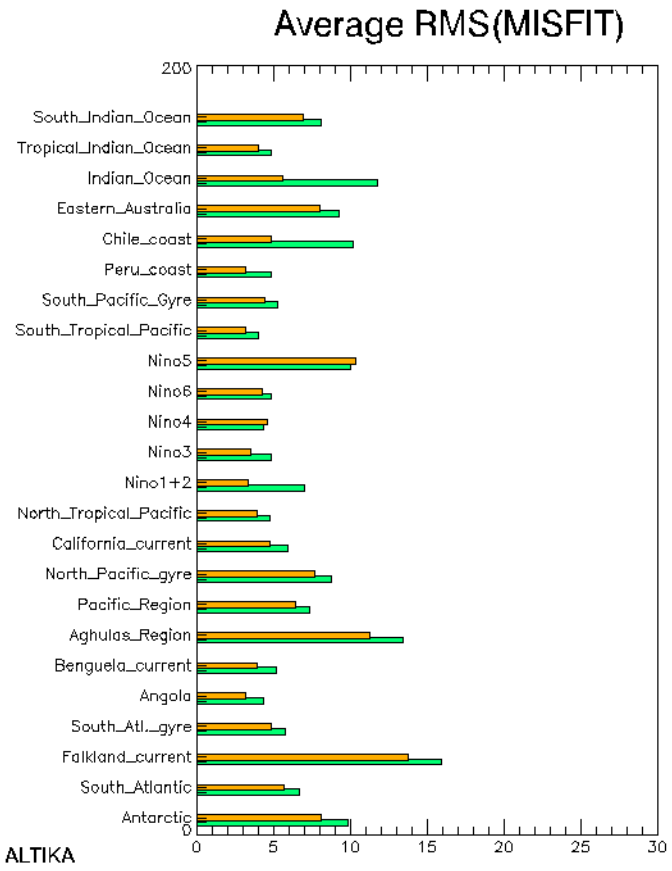

Figure 29: *Annual mean RMS error of SLA innovations over the period 2014-07-01 to 2015-09-01 for regions in the Northern Hemisphere for GIOPSv2.1(orange) and GIOPSv1.1 (green). Statistics are shown for Saral/Altika.*

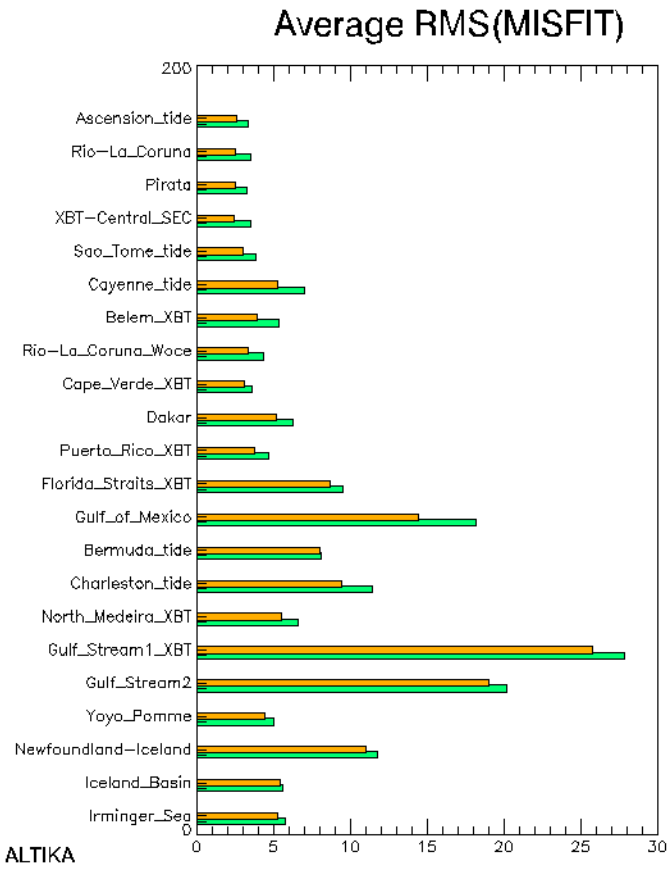

Figure 30: *Annual mean RMS error of SLA innovations over the period 2014-07-01 to 2015-09-01 for regions in the Southern Hemisphere for GIOPSv2.1 (orange) and GIOPSv1.1 (green). Statistics are shown for Saral/Altika.*

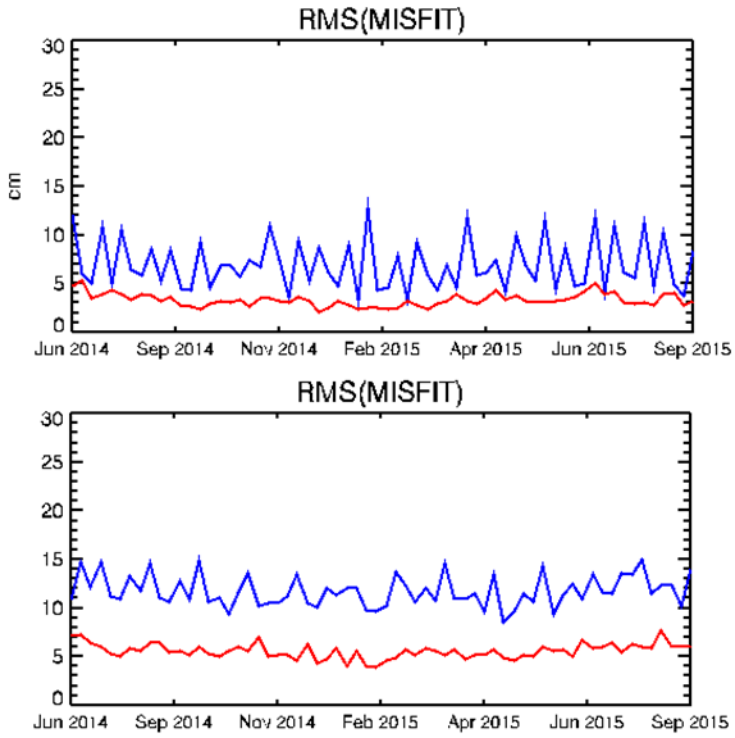

***Figure 31**: Timeseries of SLA innovation statistics for the Nino1+2 and Indian Ocean regions for GIOPSv2.1 (red) and GIOPSv1.1 (blue). Statistics are shown for Saral/Altika.*

Sea surface temperature (SST)

The RMS differences of SST innovations of GIOPSv2.1 and GIOPSv1.1 are shown in Figure 32. Note that the observation operator uses a model daily mean for day 7 when calculating innovations and that no Shapiro filter is applied to model fields. Overall, the two systems are equivalent with annual mean global RMS innovations of 0.49 and 0.48 for GIOPSv1.1 and GIOPSv2.1 respectively. However, some regional differences are present. In general, GIOPSv2.1 performs better in dynamically active regions due to the use of the IAU (i.e. equatorial Pacific). Whereas, GIOPSv1.1 shows lower RMS errors in the North Pacific and Indian Ocean due to a tighter constraint to the CCMEP SST analysis.

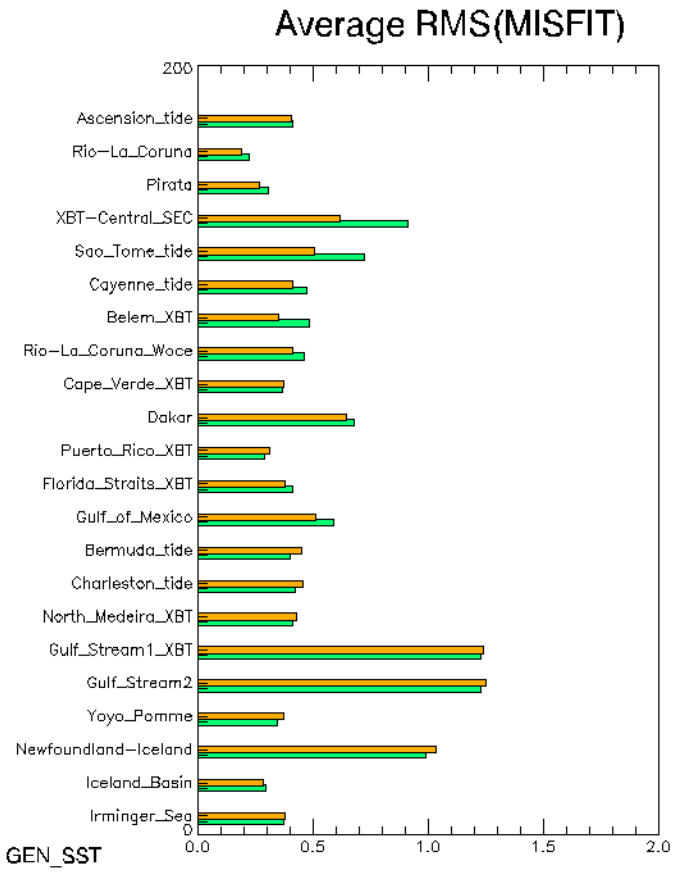

Figure 32: *Annual mean RMS error of SST innovations over the period 2014-07-01 to 2015-09-01 for regions in the Northern Hemisphere for GIOPSv2.1 (orange) and GIOPSv1.1 (green).*

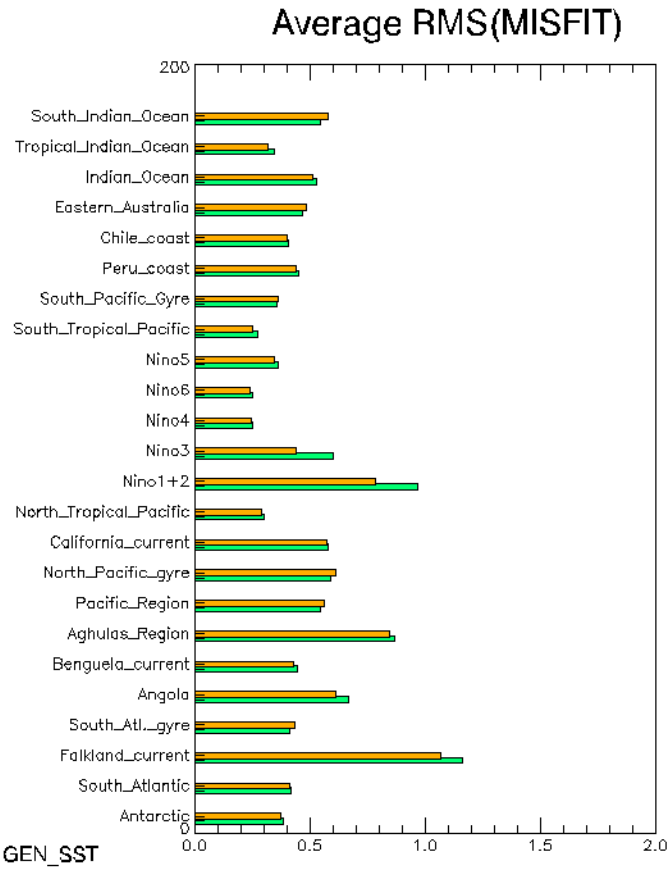

Figure 33: *Annual mean RMS error of SST innovations over the period 2014-07-01 to 2015-09-01 for regions in the Southern Hemisphere for GIOPSv2.1 (orange) and GIOPSv1.1 (green).*

In situ temperature and salinity observations

Innovation statistics for in situ temperature and salinity are shown in Figures 34-37. In situ temperature is mostly unaffected by the modifications introduced in GIOPSv2.1. A slight improvement in mixed layer depths is reflected in Figure 34 as a small reduction in RMS error around 100m depth. However, statistics for salinity profiles show an increase in RMS error in the upper 200m. This error is due to the exclusion of VP innovations when calculating the adaptivity coefficient in GIOPSv2.1. In GIOPSv1.1 significant salinity departures increased background errors leading to larger increments and reduced innovations over time. In GIOPSv2.1, as the adaptivity coefficients are calculated from only the SLA and SST innovations, a reduction in background error may be taking place in these regions resulting in the increase in

RMS salinity innovations. In the next version of GIOPS a 3DVar bias correction scheme will be implemented to address this issue.

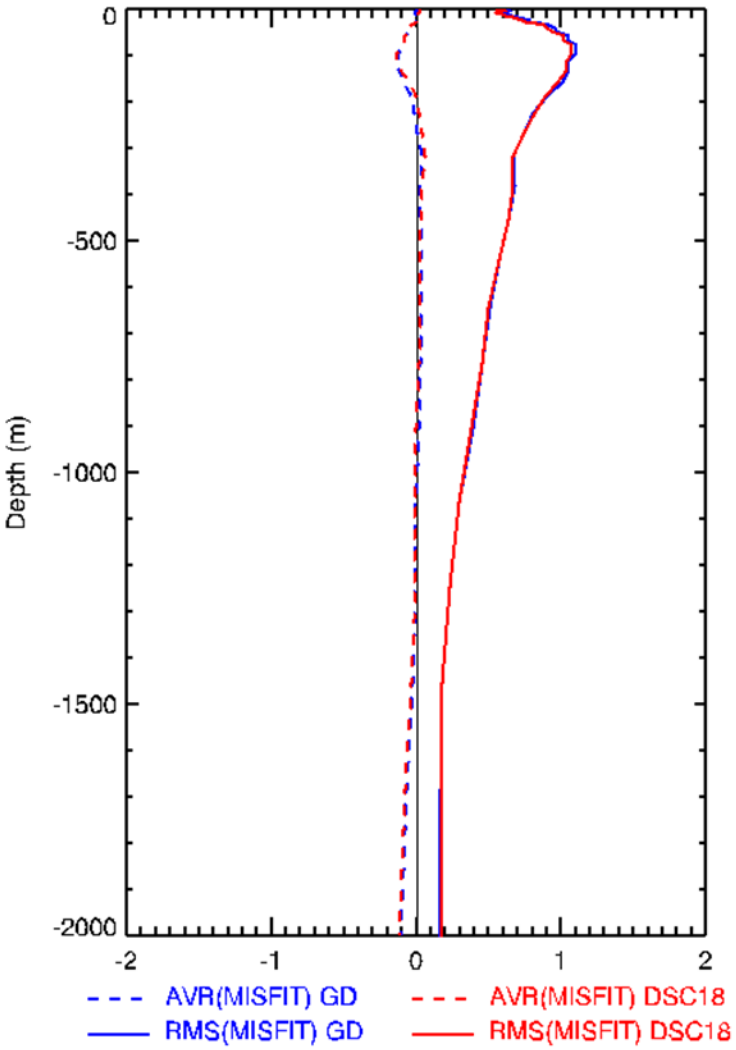

Figure 34: *Annual mean innovation statistics for in situ temperature. The mean (dashed) and RMS (solid) innovations statistics are shown for GIOPSv2.1 (red) and GIOPSv1.1 (blue). Units are in °C.*

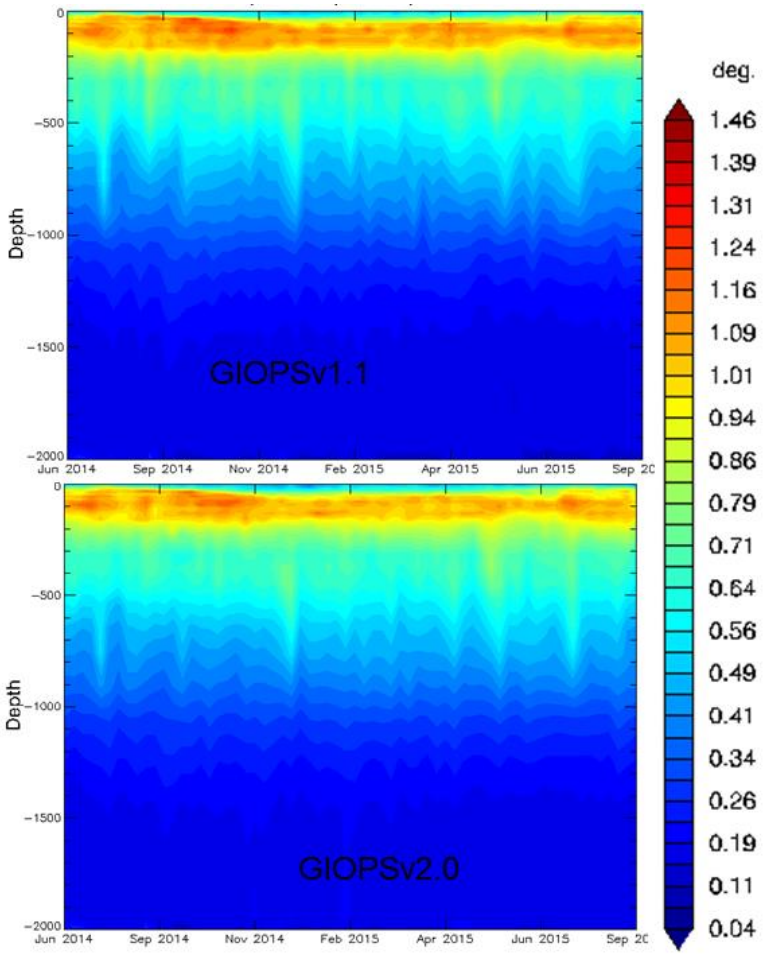

Figure 35: *Time series of RMS innovation statistics for in situ temperature. The RMS innovations statistics are shown for GIOPSv1.1 (top) and GIOPSv2.0 (bottom). Units are in °C.*

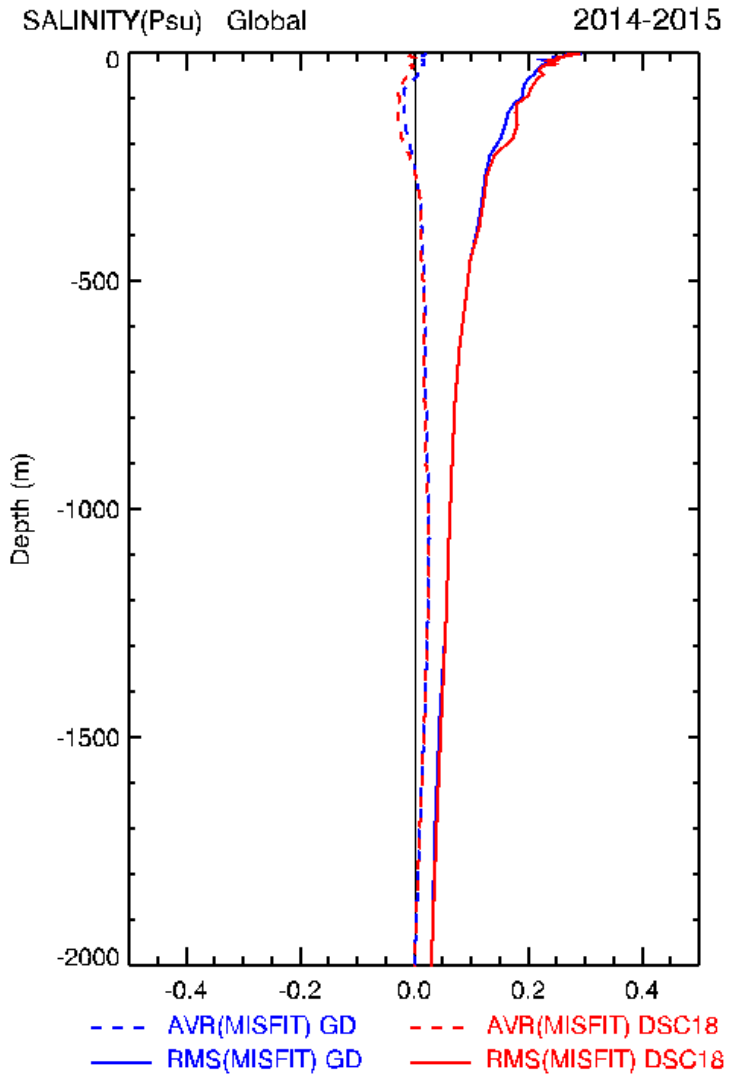

Figure 36: *Annual mean innovation statistics for in situ salinity. The mean (dashed) and RMS (solid) innovations statistics are shown for GIOPSv2.1 (red) and GIOPSv1.1 (blue). Units are in psu.*

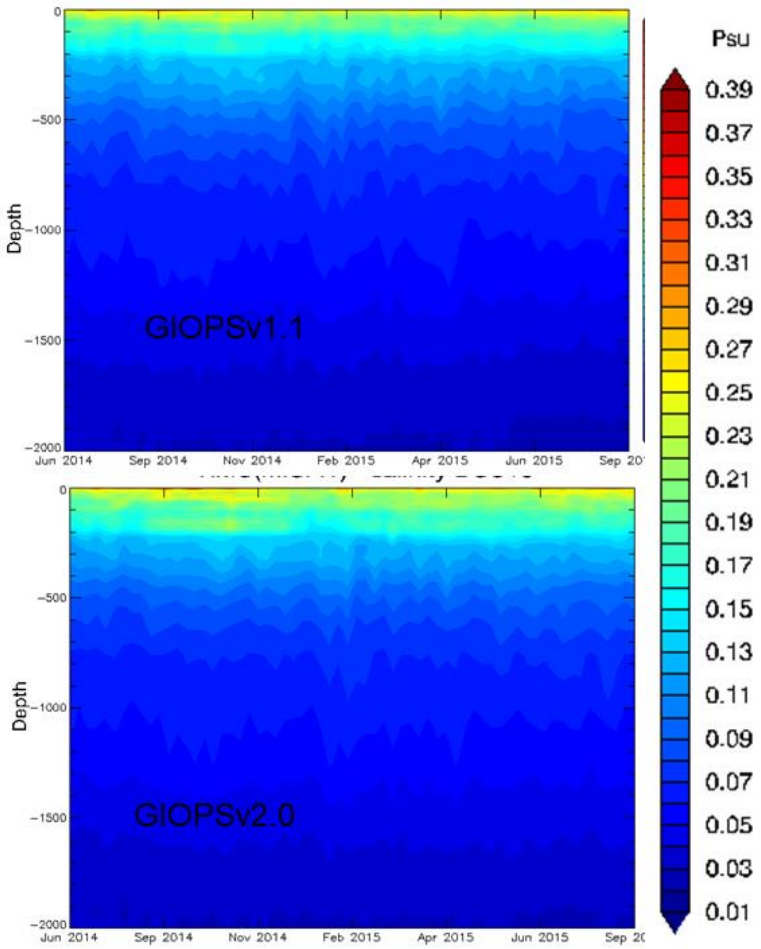

Figure 37*: Timeseries of RMS innovation statistics for in situ salinity. The RMS innovations statistics are shown for GIOPSv1.1 (top) and GIOPSv2.1 (bottom). Units are in psu.*

Comparison of SST analysis fields

An important application of GIOPS analyses is to initialize coupled atmosphere-ice-ocean forecasts. As such, it is important to minimize initialization shock and to be sure SST fields are very similar to the SST fields that the atmospheric model used during its assimilation cycle. Mean differences between GIOPS SST analyses and operational CCMEP SST analyses for GIOPSv2.1 and GIOPSv1.1 are shown in Figure 38. Since GIOPS assimilates the CCMEP SST analyses, the differences are due to the particular error statistics and methods employed and are not necessarily errors. Statistics are shown for boreal summer as this period shows the largest differences. Overall, differences are quite small and within observation error (estimated

at about 0.5°C, see Brasnett, 2008). The largest differences occur in the North Pacific Ocean and along the ice edge. The larger departures from the CCMEP SST analysis by GIOPSv2.1 is due in part to the use of the IAU. Indeed, the SST increments between GIOPSv2.1 and GIOPSv1.1 are very similar. However, part of the increment is lost due to nonlinear interactions (heat fluxes, vertical mixing) resulting in a larger difference with the CCMEP SST. This likely also occurs in GIOPSv1.1 over the first 24 hrs of the forecast.

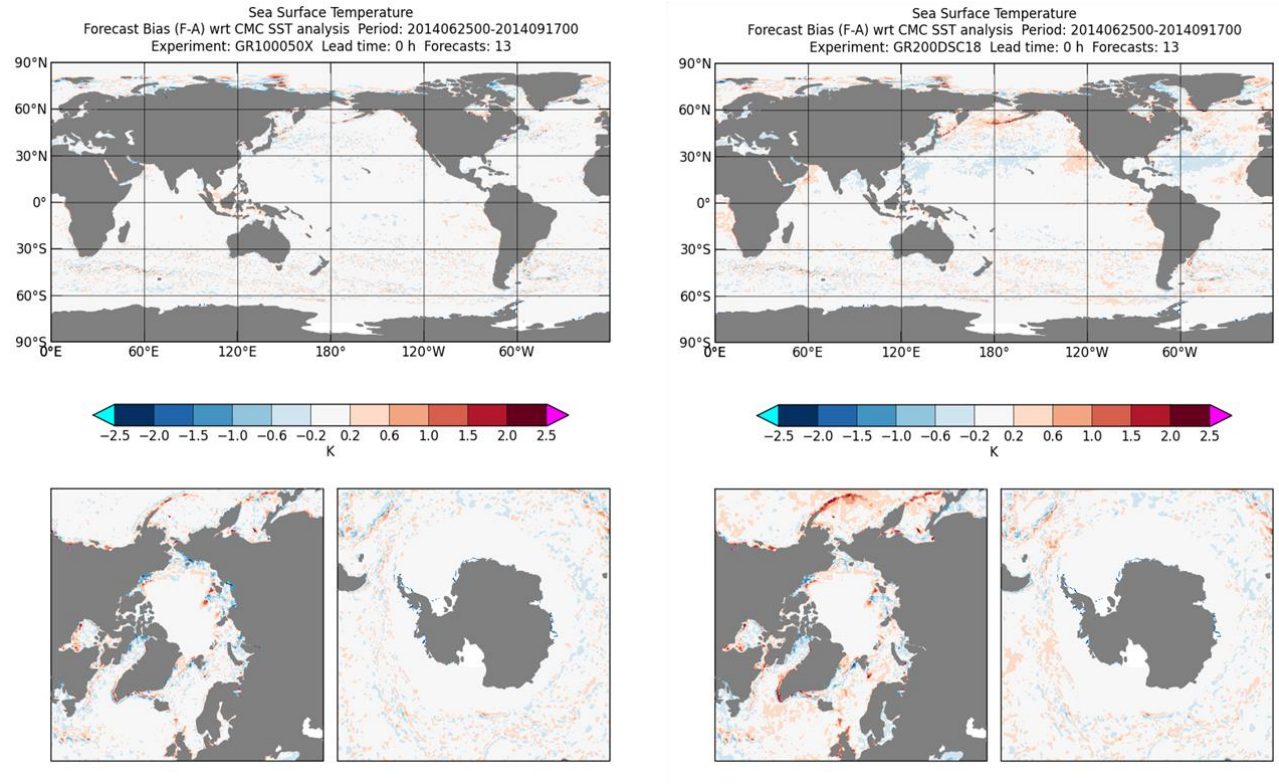

Figure 38: *Mean difference between GIOPS SST analyses and those produced operationally at CCMEP. Means are calculated using weekly GIOPS analyses over the period 2014-06-25 to 2014-09-17. This period was chosen as this is when the largest differences occur. Results are shown for GIOPSv1.1 (left) and GIOPSv2.1 (right). Differences of less than 0.2°C are shown in white.*

Verification of SST forecasts

A comparison of 7 day forecast error in GIOPSv2.0 and GIOPSv1.1 is shown in Figure 39. As noted above, only results for Boreal summer are shown as this is the period with the largest errors. In Figure 39a we see that the areas of significant ocean eddy variability are those

showing the largest error. Additionally, significant error growth is also seen in the North Pacific and Atlantic and along the Arctic ice edge. The difference in the standard deviation of the error for GIOPSv2.0 and GIOPSv1.1 is shown in Figure 39b. Here, we see that there is a reduction of error in the equatorial Pacific and Atlantic Oceans, most likely associated with the use of the IAU in GIOPSv2.0 reducing analysis shock. However, there is some increase in error in GIOPSv2.0 in some areas, in particular in the North Pacific Ocean, possibly associated with the reduced constraint toward the CCMEP analysis due to the change in the adaptivity scheme. Overall, the impact of changes introduced in GIOPSv2.0 to SST forecast skill is quite small.

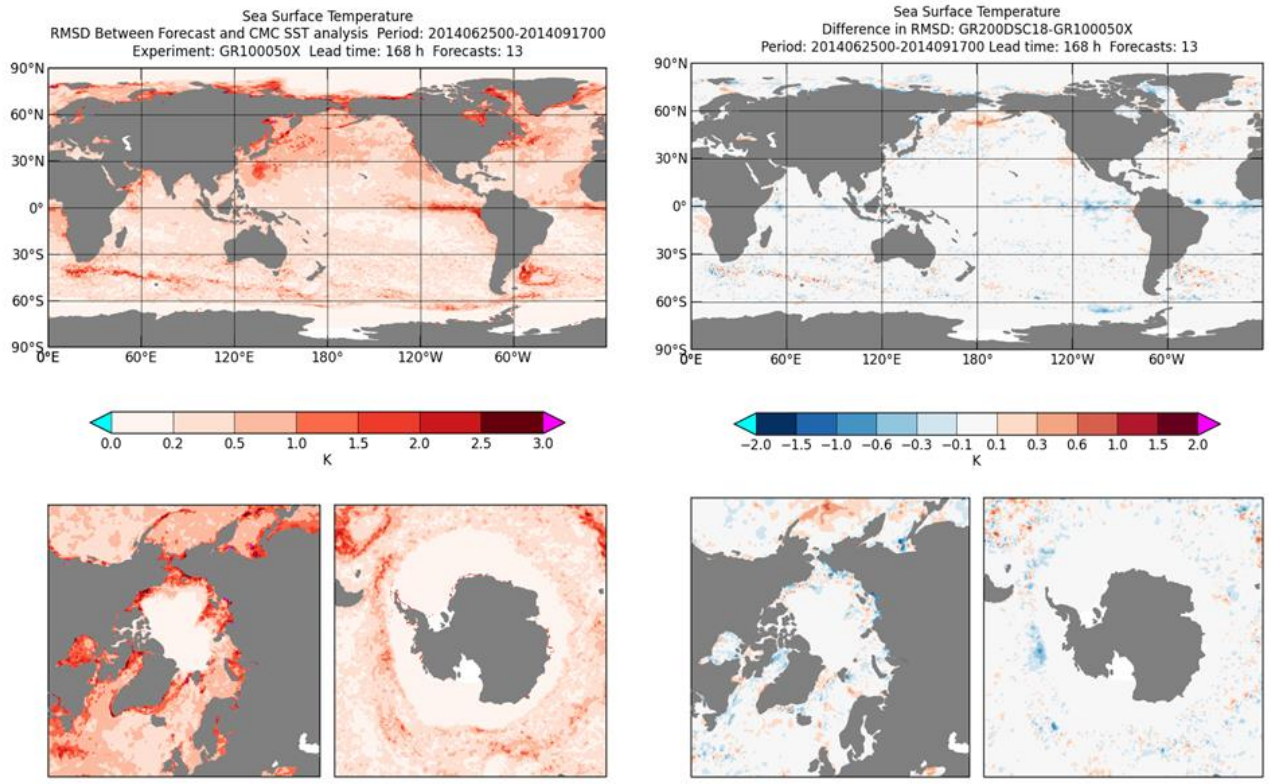

Figure 39: *SST forecast verification against the CCMEP SST analyses at a lead time of 7 days over Boreal summer (2014-06-25 to 2014-09-17). The standard deviation of differences between 7 day GIOPSv1.1 forecasts and CCMEP analyses is shown in the left panel (a). The right panel (b) shows the change in standard deviation between GIOPSv2.1 and GIOPSv1.1. Warm (cool) colours indicate larger (smaller) errors in GIOPSv2.1.*

When forecast skill is assessed by region and lead time, we can see that GIOPS produces skillful forecasts (i.e. smaller RMS error than persistence) over most regions of the ocean. Two exceptions are the tropical Atlantic and Pacific and the polar regions. In both regions, GIOPS forecasts have lower RMS than persistence of GIOPS analyses, but have larger mean error than persistence of CCMEP analyses. Further investigation of these errors is underway using additional independent observations.

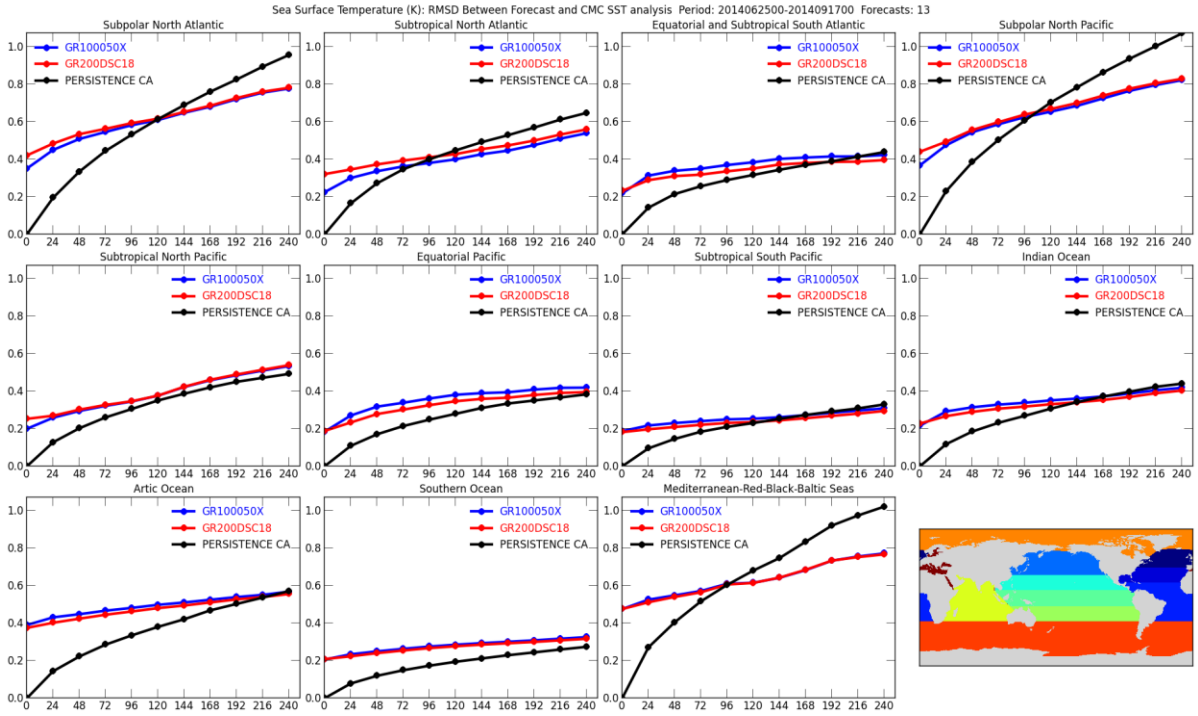

Figure 40: *SST forecast verification against the CCMEP SST analyses as a function of lead time over 11 sub-regions for Boreal summer (2014-06-25 to 2014-09-17). The standard deviation of differences for forecasts from GIOPSv1.1 (blue) and GIOPSv2.1 (red) and CCMEP analyses is shown as well as the standard deviation of differences for persistence of the CCMEP analyses. A 21-pass Shapiro filter is applied to GIOPS fields prior to comparison with CCMEP analyses.*

Conclusion

The Global Ice Ocean Prediction System is a comprehensive analysis and forecasting system capable of providing high quality products. GIOPS produces daily analyses and 10-day forecasts on a 1/4° resolution global grid. Ocean analyses show very good agreement with sea level anomaly, sea surface temperature and in situ temperature and salinity observations. Overall, the system performs similarly to the equivalent system running at Mercator-Ocean (PSY3V3R2). Modifications to the SST assimilation appear to have significantly improved SST analyses as compared to Mercator. This is due in particular to the assimilation of CCMEP SST operational analyses in place of NCEP-RTG analyses (as is done my Mercator), together with reduced observational errors and changes to the SST observation operator and treatment along the ice edge. These modifications have allowed GIOPS to produce SST analysis that agree with CCMEP analyses to within estimated errors (0.3°C). The largest area of disagreement is along the ice edge, where GIOPS is systematically colder than the CCMEP SST analyses.

Sea surface temperature forecasts show systematically lower errors than persistence of either GIOPS analyses or CCMEP operational analyses. Areas of particular skill are found near and downstream of the Kuroshio Current and Gulf Stream. The former results in a large gain in RMS forecast skill as compared to persistence. The primary error in SST forecasts appears to be related to positive biases in shortwave radiation from the GDPS. It is not clear the relative contribution of radiation errors associated with model spin up, overly transparent clouds and an insufficient representation of marine stratocumulus clouds. Another area of SST forecast error exists along the ice edge where GIOPS appears to have a cold bias in both its analysis and forecasts. Improvements to the assimilation scheme are underway to address this.

GIOPS establishes the foundation for a marine core service within Canada. The GIOPS analysis products can be used to provide initial conditions for both regional ice-ocean forecasting systems as well as monthly to seasonal forecasts. GIOPS forecasts can be used in R&D to evaluate potential benefits associated with inclusion of a time-variable bottom marine boundary condition for atmospheric forecasts. Moreover, GIOPS products support a variety of needs within the Government of Canada for marine emergency response, marine safety and

security, and ecological management. This Canadian marine core service will also support a growing industrial and commercial need for accurate marine information products.

Annex C - Task 3: Technical Report: Verification

GIOPS / CECOM Comparison

We provided an objective comparison and validation against observations (i.e. Class 4 Metrics) for both CECOM and GIOPS ocean prediction systems in northwest Atlantic and Arctic regions with different temporal periods for year 2013. This was done to develop the inter-comparison metrics and tools to be used for all other forecasts systems in development by CONCEPTS including the high resolution system for the Grand Banks. As a 10-day global prediction system with 1/4 degree resolution and data assimilation, GIOPS shows prediction performance skill as good as CECOM's which is a 2-day regional forecasting system with 1/10 degree resolution with limited assimilation/incorporation of data. For sub-surface temperature, sea level anomaly and sea ice total concentration, GIOPS has lower error than CECOM.

We have compared quantitatively the performance of these two models in pre-defined sub-areas. Forecasting of ocean conditions in the Gulf Stream ocean is most difficult with highest RMSE values for temperature, salinity, and sea level anomaly. In this area though, GIOPS outperforms CECOM due to assimilation of altimeter data that constrains Gulf Stream Eddies to be in the right location. Thus it is not surprising that GIOPS has a better fit, which demonstrates importance of data assimilation for SLA.

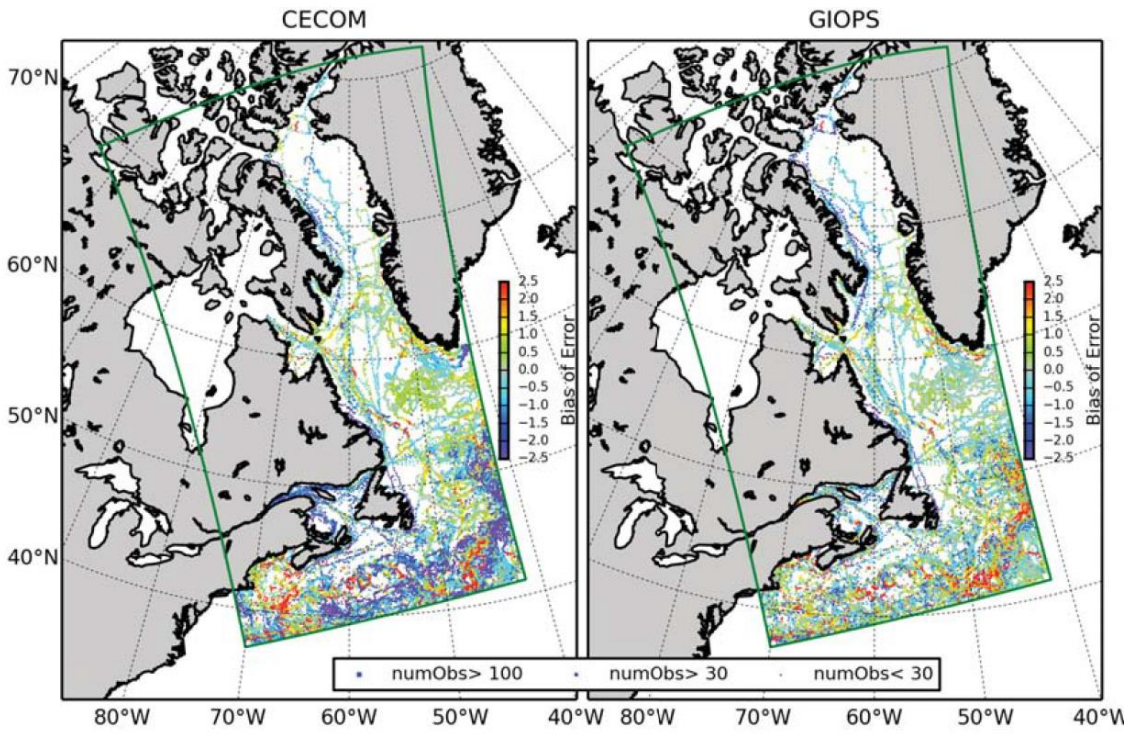

Figure 41: *Bias of temperature misfit for year 2013 (difference between modelled and observed in-situ Sea Surface Temperature) for CEOM (left) and GIOPS (right). The misfits were gridded over 0.1 x 0.1 degree cells. The size of the dots indicate number of observations in each cell. The figure shows the impact of data assimilation present in GIOPS in reducing model error. This is noticeable particularly in shelf break areas as well as the Gulf Stream.*

In general, it is our expectation that CECOM should perform better than GIOPS in coastal and shelf regions due to its higher horizontal resolution and depth dependent (model vertical resolution is a function of water depth, also known as sigma coordinates) coordinate vertical representation. GIOPS is global model with vertical levels varying in thickness from 1m to 400m. GIOPS however does show equal or similar skill scores as CECOM even in shelf regions.

Furthermore we have observed there are similar misfits on shelf for both system in temperature, salinity, and sea surface height. These localized features which are not represented by either of these two systems, could be related to particular observations which might not be representative. In order to properly constrain sub-surface properties on the shelf,

a regional system that assimilates these data in real time is necessary, which includes in situ temperature/salinity profiles, as well as near shore satellite sensed sea level anomaly (SLA) data.

The compared prediction systems make use of two different numerical ocean models as well as two different numerical ice models. The prediction systems were developed for different purposes. CECOM has been widly used by industries, and CECOM is regional ocean forecast system that is initialized from climatology but forced with real time atmospheric forecasts. GIOPS is a newer system, and GIOPS is a global ocean ice prediction system is initialized from daily ocean surface and weekly full 3D analysis of the ocean. There is a systematic difference in the assimilation of these two systems. One may argue that comparing two different ocean prediction systems using different assumptions on ocean behavior (i.e. models) may not provide a clear comparison. However comparing two ocean prediction systems to the same observed data set allows us to evaluate how good output from both forecast systems are (despite their obvious differences) at recreating observations. This furthermore allows us to extract the advantages and disadvantages of each system in reproducing the same observed data set and also provides a quantitative performance assessment to end users.

Drifter Deployment and Program

To increase the amount of data available for ocean forecast output verification a drifter program component was initiated. A total of 50 surface ISVP drifter were purchased and deployed between Juley 2015 and September 2016 covering the NL shelves (see Figure 42 below). Numerous verifications were done with this drifter set.

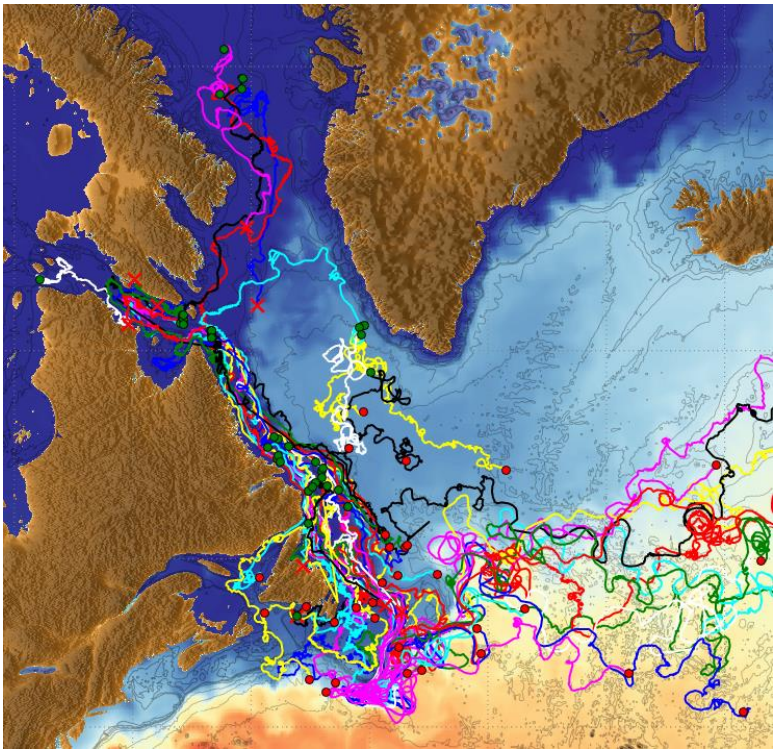

Figure 42: *Tracks of 50 drifters deployed on the NL shelves and upstream between Summer 2015 and Summer 2016 drifting up to March 14th 2017. Drifters collected sea surface temperature, barometric pressure and position. Drifter data can be accessed from http://navigator.oceansdata.ca.*

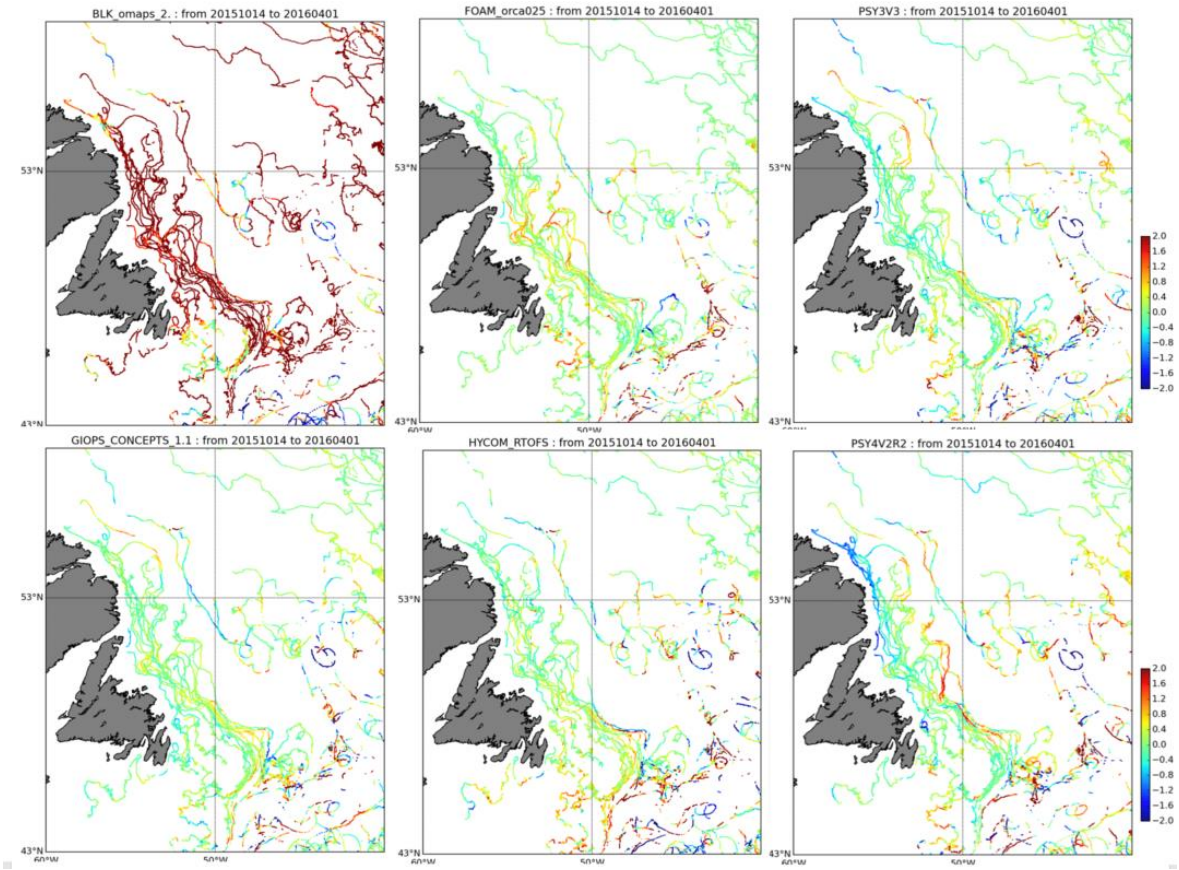

Figure 43: *Surface Temperature difference between 6 international ocean prediction systems and observed drifters deployed in the North West Atlantic from 2015-06 to 2016-04. The GIOPS prediction system is shown in the bottom left panel. Other systems include the Australian OMAPS system (top left), the UK FOAM Forecasting System (top middle), the French PSY3 system (top right), the US HYCOM system (bottom middle) and the French 1/12th degree PSY4 system (bottom right). These types of comparisons will be done routinely for the CIOPS prediction system.*

Annex D - Task 4: Technical Report: Implementation of forecast system to operations:

A high-resolution (1/36°) NEMO-CICE ocean forecast maestro suite of Grand Banks region (CIOPS/GBN36/CREG36) has been set up on Environment and Climate Change Canada (ECCC) super computer network, based on the domain configuration of Task #1. A 3-month simulation for 2014 summer (June 1st to August 31st) was carried out with this configuration to test the capability of this model in a user account.

The ocean component of the model is updated to CONCEPTS version 3.1.2 (based on the NEMO version 3.1, Madec, 2008), so it is ready to run on the new generation of High Performance Computing (HPC) platform at ECCC. CORE bulk formula (Large and Yeager, 2004) is used to calculate fluxes.

The sea-ice component of the model is based on the Community Ice CodE (CICE) version 4 (Hunke, 2001; Hunke and Lipscomb, 2010).

The bathymetry of CIOPS is derived from the block-median of SRTM30_Plus data, which is the global bathymetry and elevation data at 30 arcsec resolution (Becker et al., 2009; Sandwell et al., 2014).

Daily Global Physical Bulletin at 1/12° (PSY4, Gutknecht et al., 2015) data from Mercator Ocean operational system is used to initialize and force the open boundaries (North, South, East and West) of our 3-month hindcast. We also use the PSY4 data as the spectral nudging (Thompson et al., 2006) target in this experiment (only the spatial filter is used, i.e. the large scale are nudged (>120 km) but the smaller scales are free to evolve), following the same approach as in the Regional Ice Ocean Prediction System (RIOPS) which itself targets the Global Ice Ocean Prediction System (GIOPS).

The model is forced by tides at the four boundaries via a Flather boundary condition on the barotropic flow. The five major harmonic constituents of the regional are used: M2, N2, S2, K1,

O1. They are taken from the OSU TOPEX/Poseidon Global Inverse solution TPXO 7.2 (Egbert et al., 1994; Egbert and Erofeeva, 2002). The model also computes a tidal astronomical forcing that is applied over the whole domain. In the deep ocean the tides tend to have marginal impact but on the shallow region of shelf and banks, they are determinant in reproducing the correct amount of vertical mixing.

The atmospheric forcing is from ECCC's latest Regional Deterministic Prediction System (RDPS, Caron et al., 2015) and Global Deterministic Prediction System (GDPS, Buehner et al., 2015). The RDPS has a spatial resolution of 10km but it does not cover the whole CIOPS domain, so we have blended the coarser (25km) GDPS data to forcing our model. For each day, hourly forecast on 00Z and 12Z (6-17h) are used to drive the model.

For future use of CIOPS in operations, we have prepared a provision for switching the spectral nudging target to RIOPS forecast, which is run at ECCC operationally since June 2016.

CIOPS is meant to run operationally at ECCC. However, ECCC is in the process of migrating all of its weather & environmental prediction capacities to a new supercomputer solution. During this period (until the end of the summer), it is highly recommended to not add to the burden of the teams involved, and therefore CIOPS will be maintained in the meantime in a user account. When the migration is completed, new developments would be welcome to be proposed and implemented, including CIOPS. We are therefore hopeful that by fall 2017 CIOPS can be proposed to run operationally.

Spectral nudging implementation and impact

The spectral nudging implementation in CIOPS is based on the original code of Thompson et al., (2006) with this specific setup: the temporal filter is disabled in favor of using solely the spatial filter (a simple repetitive Shapiro filter). After some trial and errors, we decided to go with a maximum number of 60 repetitive passes in the Shapiro filter, which is equivalent to a nominal 2 km * 60 = 120km low pass filter. The time relaxation parameter in the nudging term is set to one day, which is quite a short time for relaxation (generally models use value of 30 days) but is necessary in the present configuration if one is to take full advantage of the data assimilation

done in the target model. The fundamental idea of spectral nudging remains the same though: the low pass nudging (in time or in space domain) – or spectral nudging as it is called— constrains the long wave characteristics of the flow but allows smaller scales to evolve more or less freely (depending on the quality of the filtering procedure).

To illustrate the effect of nudging, we compare the field of temperature gradient magnitude at 92m (vertical level 22) after 3 month of simulation in Fig. 1 for the target data-assimilative model (PSY4), a version of CIOPS with standard nudging instead of spectral nudging and the present version of CIOPS (with spectral nudging). The gradient of temperature is very informative of the level of details that the model can reproduce, i.e., the effective model resolution. Clearly, the version with standard nudging is gives very similar results to the target model, which is expected, given the strong nudging applied. This also means however that the effective resolution is not around 2 km as intended but more that of the driving model which is 6 km. Hence, very little gain is made by nudging the standard way a high resolution regional model to the driving data assimilative model. On the other hand, the present CIOPS configuration with spectral nudging allows a much finer level of representation and at the same time the large scale features of the flow of the driving model are reproduced. And presumably, the accuracy of the data-assimilative model resides in the large scale flow since oceanic observations are still too sparse to allow for high resolution data assimilation.

Another interesting metric is the time evolution of the domain-averaged magnitude of temperature gradient. Figure 2 shows this evolution for again the target model PSY4, a version of CIOPS with standard nudging instead of spectral nudging and the present version of CIOPS. The latter has a level of magnitude higher than the two former ones by approximately 30%. It is noteworthy that this increase happens quite quickly in the first 5 days of ramping the model from the target solution. The added value of the spectral nudge comes therefore rather quickly, likely through baroclinic instabilities of the flow.

Lastly, a spectrum analysis is performed for a particular latitudinal line of the domain, here taken when the horizontal index of the grid is equal to 500, which happens to be just east of Flemish Cap, and at a depth of 92 m for a version of CIOPS with standard nudging and the

present version of CIOPS with spectral nudging. The spectral analysis is done in the time domain (in this case, an average of spectra is done spatially along the latitudinal line) or in the space domain (then an average in time is done for all spatial spectra for the period June 1st to August 30th, 2014). The spectral analysis (Fig. 3) highlights the expected result that the spectral nudging in CIOPS allows to reproduce the variability of the coarser driving model down to 50 km (in space) and a month (in time) and that beyond the model is able to generate its own variability. In contrast, the spectrum of the model strongly relaxed to the driving model dips more quickly as the internal variability is suppressed even at high resolution.

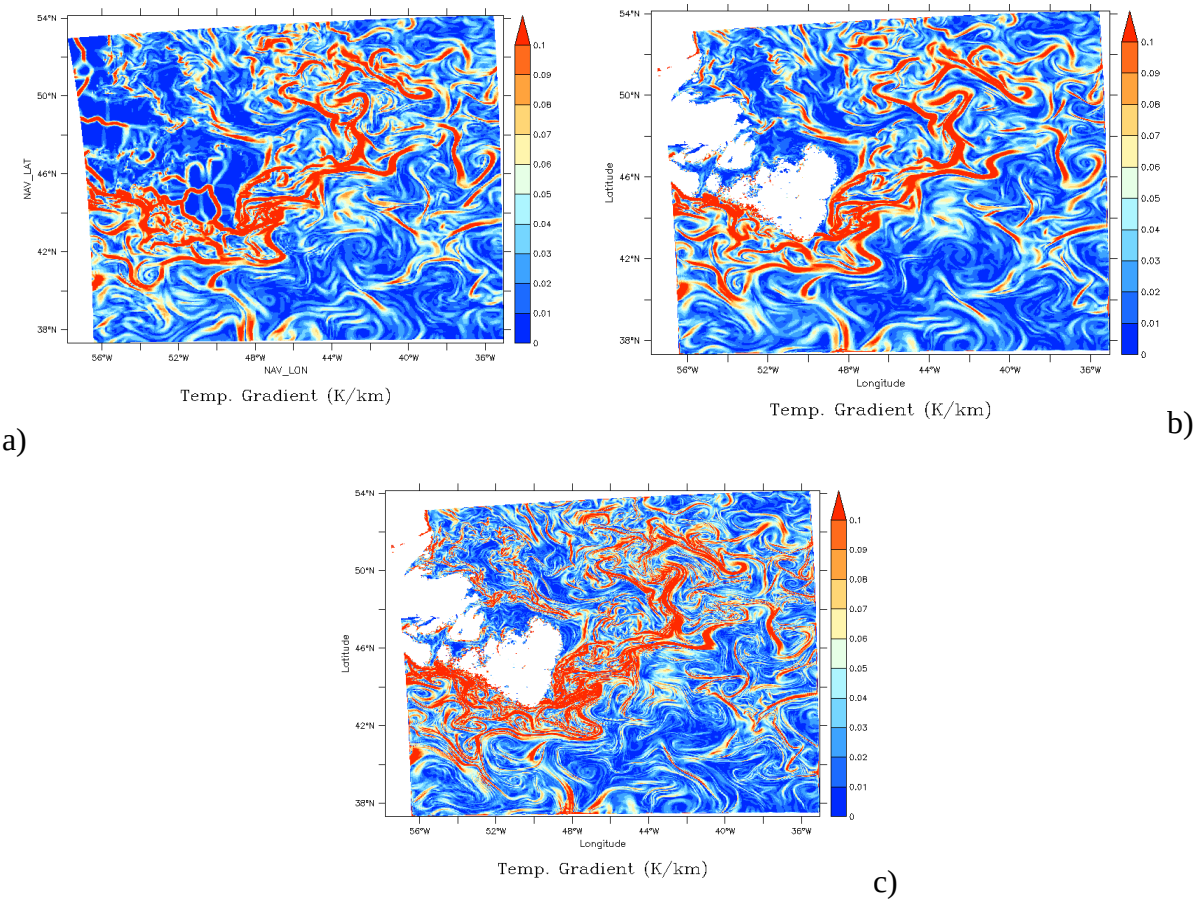

Figure 44: magnitude of the temperature gradient at 92m in K/km on August 30th 2014 of the target model PSY4 (a) interpolated to the regional grid (note that values over the Grand Banks and land are actually derived from extrapolation), the regional model with tides and standard nudging (b) and the regional model with tides and spectral nudging (c) with 60 repetitive passes of the Shapiro filter.

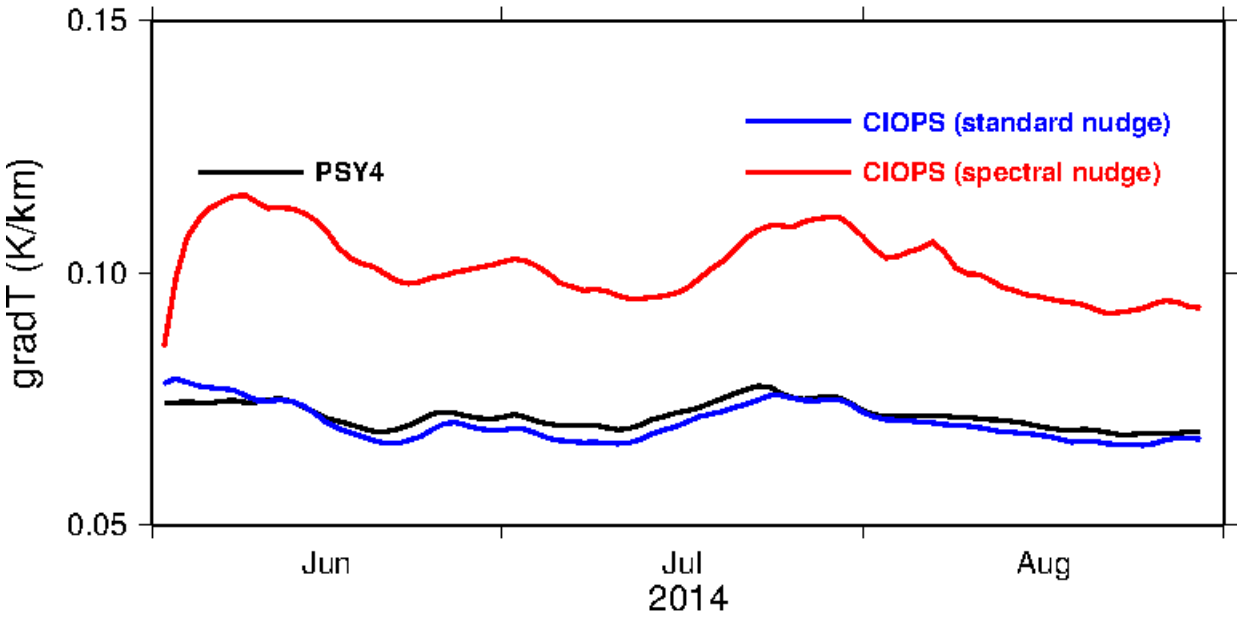

Figure 45 : History of the evolution of the domain averaged magnitude of the temperature gradient for the target model (black), a version of the regional model with standard nudging (blue) and the present CIOPS configuration (red) at 92 m.

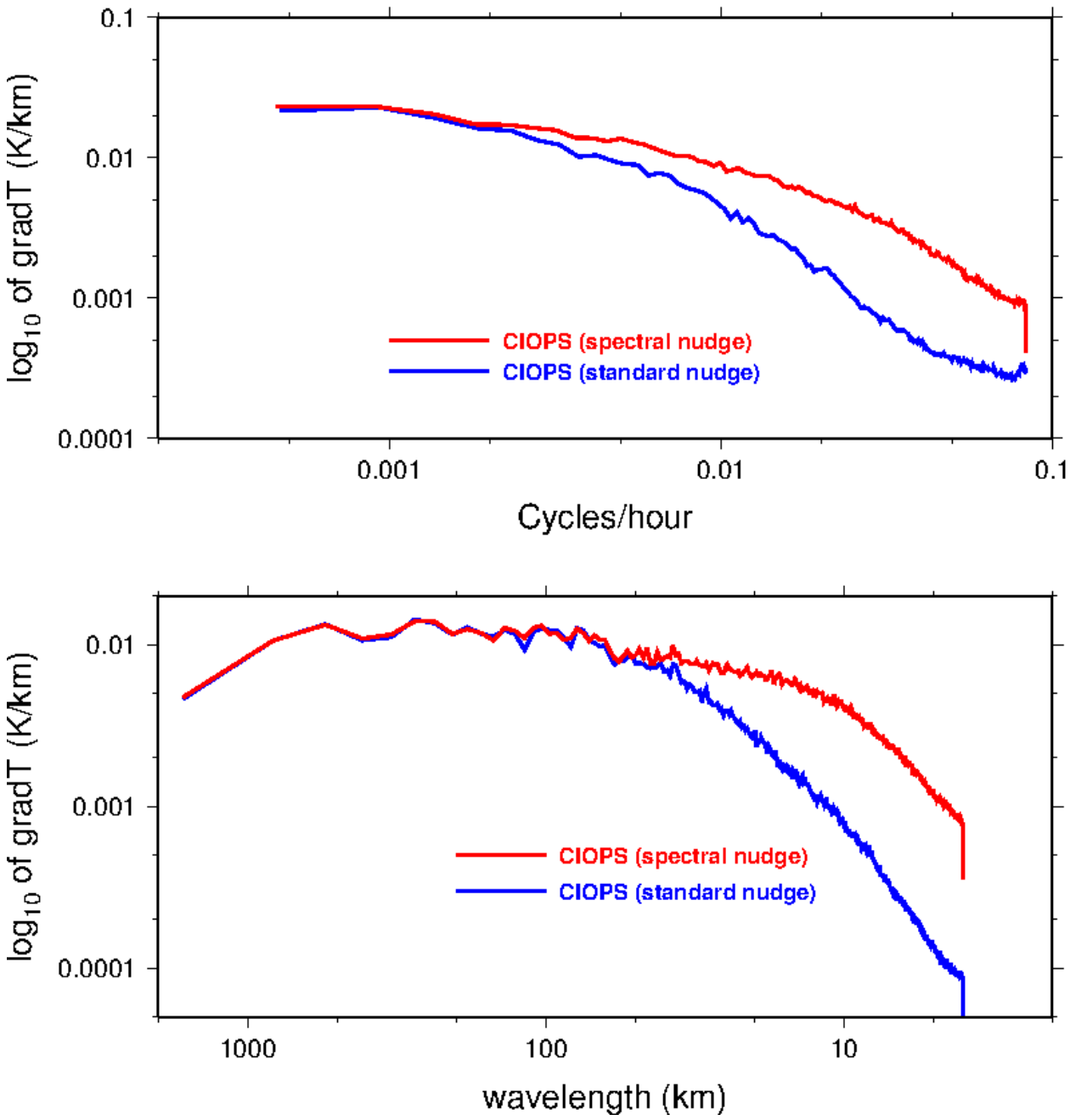

Figure 46: Spectrum analysis of temperature gradient for a version of CIOPS with standard nudging and the present version with spectral nudging along the 500th i-point of the domain at 92 m deep. The top panel is the spectrum in the time domain (spatial average of all point lying along the 500th i-line) and the bottom panel is the spectrum in the space domain along the 500th i-line (temporally averaged).

Annex E - Task 5: Technical Report: Implementation of operational dissemination system

Technical Description

Ocean Navigator is a Data Visualization tool that enables users to discover and view 3D ocean model output quickly and easily.

The ocean model output is stored in NetCDF files. These files are self-describing and contain the 2D or 3D model output for one or more timesteps and one or more variables.

To facilitate reading all these files, we make use of a server called THREDDS Data Server. THREDDS aggregates all the NetCDF files and allows users to query subsets of the files.

The server-side component of the Ocean Navigator is written in Python, using the Flask web API. Conceptually, it is broken down into three components:

Query Server

This portion returns metadata about the selected dataset in JSON format. These queries include things like the list of variables in the dataset, the times covered, the list of depths for that dataset, etc.

These queries are generally fast as this data is cached in the THREDDS server, avoiding the need to scan through the NetCDF files.

The other queries include things such as predefined areas (NAFO divisions, EBSAs, etc), and ocean drifter paths. The drifter paths are loaded from NetCDF files, but all the other queries are loaded from KML files.

Plotting

This portion generates an image plot, which could be a map with surface fields (or fields at a particular depth), a transect through a defined part of the ocean, depth profiles of one or more points, etc. We use the matplotlib python module to generate the plots.

Because the model grid rarely lines up with the map projection, and profiles and transects don't necessarily fall on model grid points, we employ some regridding and interpolation to generate these plots. For example, for a map plot, we select all the model points that fall within the area, plus some extra around the edges and regrid to a 500x500 grid that is evenly spaced over the projection area. An added benefit of this regridding is that we can directly compare across models with different grids. This allows us to calculate anomalies on the fly by comparing the model to a climatology. In theory, this would also allow for computing derived outputs from variables in different datasets with different native grids.

Tile Server

This portion is really a special case of the plotting component. The tile server serves 256x256 pixel tiles at different resolutions and projections that can be used by the OpenLayers web mapping API. This portion doesn't use matplotlib, as the tiles don't have axis labels, titles, legends, etc. The same style of interpolation/regridding is done to generate the data for the images.

The generated tiles are cached to disk after they are generated the first time, this allows the user request to bypass accessing the NetCDF files entirely on subsequent requests.

The user interface is written in Javascript using the React framework. This allows for a single- page, responsive application that offloads as much processing from the server onto the user's browser as possible. For example, if the user chooses to load points from a CSV file, the file is parsed in the browser and only necessary parts of the result are sent back to the server for plotting.

The main display uses the OpenLayers mapping API to allow the user to pan around the globe to find the area of interest. It also allows the user to pick an individual point to get more information about, draw a transect on the map, or draw a polygon to extract a map or statistics for an area.

Component Diagram

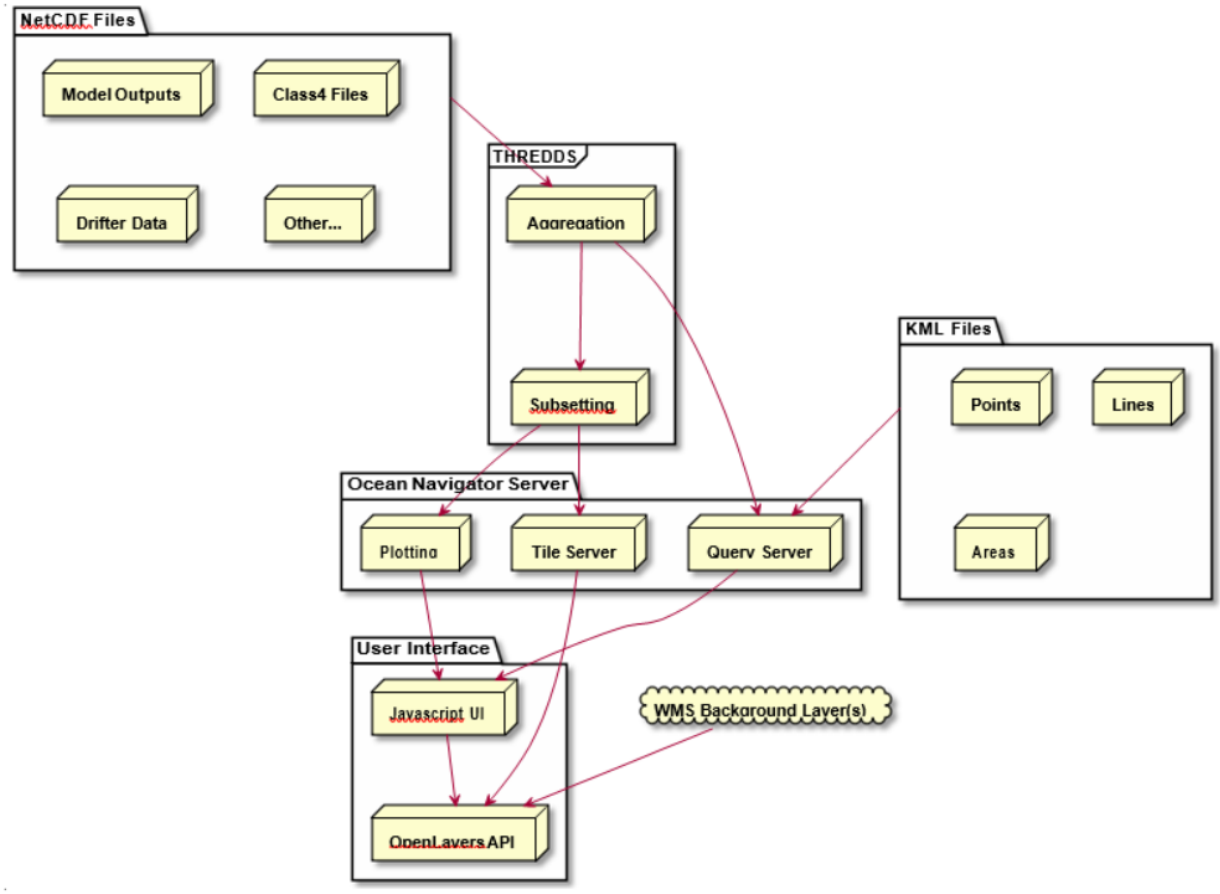

Ocean Navigator Links:

Ocean Navigator Manual: https://dfo-ocean-navigator.github.io/Ocean-Navigator-Manual/

Ocean navigator software code: https://github.com/DFO-Ocean-Navigator/Ocean-Data-Map-Project

Ocean Navigator Bug Reporting Page: https://github.com/DFO-Ocean-Navigator/Ocean-Data-Map-Project/issues

THREDDS Data Server: https://www.unidata.ucar.edu/software/thredds/current/tds/

References

Adcroft, A., C. Hill, and J. Marshall, 1997: Representation of topography by shaved cells in a height coordinate ocean model, Mon. Weather Rev., 125, 2293-2315.

Barnier, B., G. Madec, and co. authors, 2006: Impact of partial steps and momentum advection schemes in a global ocean circulation model at eddy permitting resolution, Ocean Dynamics, doi:10.1007/s10236-006-0082-1.

Barnier, B. and the DRAKKAR Group, 2007: Eddy-permitting ocean circulation hindcasts of past decades. Clivar Exchanges, 12(3): 8–10.

Becker, J. J., D. T. Sandwell, W. H. F. Smith, J. Braud, B. Binder, J. Depner, D. Fabre, J. Factor, S. Ingalls, S-H. Kim, R. Ladner, K. Marks, S. Nelson, A. Pharaoh, R. Trimmer, J. Von Rosenberg, G. Wallace, P. Weatherall., Global Bathymetry and Elevation Data at 30 Arc Seconds Resolution: SRTM30_PLUS, Marine Geodesy, 32:4, 355-371, 2009.

Blanke B, and P. Delecluse, 1993: Variability of the Tropical Atlantic Ocean Simulated by a General Circulation Model with Two Different Mixed-Layer Physics. J. Phys. Oc. 23: 1363–1388.

Brasseur, P., P. Bahurel, L. Bertino, F. Birol, J.M. Brankart, N. Ferry, S. Losa, E. Remy, J. Schröter, S. Skachko, C. E. Testut, B. Tranchant, P.J. Van Leeuwen, and J. Verron, 2005:, Data assimilation in operational ocean forecasting systems: The MERCATOR and MERSEA developments. Q. J. R. Met.Soc. 613, C, pp 3561-3582(22).

Buehner, M., McTaggart-Cowan, R., Beaulne, A., Charette, C., Garand, L., Heilliette, S., Lapalme, E., Laroche, S., Macpherson, S.R., Morneau, J. and Zadra, A., 2015. Implementation of deterministic weather forecasting systems based on ensemble–variational data assimilation at Environment Canada. Part I: The global system. Monthly Weather Review, 143(7), pp.2532-2559.

Böning, C. W., and R. G. Budich, 1992: Eddy Dynamics in a Primitive Equation Model: Sensitivity to Horizontal Resolution and Friction. J. Phys. Oceanogr., 22, 361–381.

Caron, J.F., Milewski, T., Buehner, M., Fillion, L., Reszka, M., Macpherson, S. and St-James, J., 2015. Implementation of deterministic weather forecasting systems based on ensemble–variational data assimilation at Environment Canada. Part II: The regional system. Monthly Weather Review, 143(7), pp.2560-2580.

Clarke, R. A., H. W. Hill, R. F. Reiniger, and B. A. Warren, 1980: Current System South and East of the Grand Banks of Newfoundland. J. Phys. Oceanogr., 10, 25–65.

Davidson, F., G. C. Smith, Y. Lu and S. Woodbury, 2013: Operational atmosphere-ocean-ice prediction systems in Canada: Providing decision-enabling marine environmental information to end users. Canadian Ocean Science Newsletter, March 2013, 70, pp2-5.

Dupont, F., Higginson, S., Bourdallé-Badie, R., Lu, Y., Roy, F., Smith, G. C., Lemieux, J.-F., Garric, G., and Davidson, F., 2015. A high-resolution ocean and sea-ice modelling system for the Arctic and North Atlantic Oceans, Geosci. Model Dev. Discuss., 8, 1-52, doi:10.5194/gmdd-8-1-2015.

Divakaran, P., Brassington, G. B., Ryan, A. G., Regnier, C., Spindler, T., Mehra, A., Hernandez, F., Smith, G., Liu, Y., and Davidson, F.: GODAE OceanView Class-4 Inter-comparison for the Australian Region, J. Operational Oceanogr., accepted.

Engedahl H., 1995: Use of the flow relaxation scheme in a three-dimensional baroclinic ocean model with realistic topography. Tellus, 365-382.

Egbert, G. D., A. F. Bennett, and M. G. G. Foreman, 1994: TOPEX/Poseidon tides estimated using a global inverse model. J. Geophys. Res, 99, 24821–24852.

Egbert, G.D. and Erofeeva, S.Y., 2002. Efficient inverse modeling of barotropic ocean tides. Journal of Atmospheric and Oceanic Technology, 19(2), pp.183-204.

Fu, L.-L. (1983), On the wave number spectrum of oceanic mesoscale variability observed by the SEASAT altimeter, J. Geophys. Res., 88(C7), 4331–4341, doi:10.1029/JC088iC07p04331.

Flather RA (1976) A tidal model of the Northeast Pacific. Atmosphere-Ocean 23:22–45.

Gutknecht, E., Reffray, G., Drillet, Y., Gehlen, M. and Pinazo, C., 2015. High resolution operational physical/biogeochemical coupled model systems developed at Mercator Océan. Mercator Océan, Laboratoire des Sciences du Climat et de l'Environnement, France

Hernandez, F., E. Blockley, G. B. Brassington, F. Davidson, P. Divakaran, M. Drévillon, S. Ishizaki, M. Garcia-Sotillo, P. J. Hogan, P. Lagemaa, B. Levier, M. Martin, A. Mehra, C. Mooers, N. Ferry, A. Ryan, C. Regnier, A. Sellar, G. C. Smith, S. Sofianos, T. Spindler, G. Volpe, J. Wilkin, E. D. Zaron, and A. Zhang (2015), Recent progress in performance evaluations and near real-time assessment of operational ocean products. J. Operational Oceanography 8, s221-s238, doi: 10.1080/1755876X.2015.1050282.

Higginson, S., K. R. Thompson, J. Huang, M. Véronneau, and D. G. Wright, 2011. The mean surface circulation of the North Atlantic subpolar gyre: A comparison of estimates derived from new gravity and oceanographic measurements, J. Geophys. Res., 116, C08016, doi:10.1029/2010JC006877.

Hollingsworth A, Kalbers P, Renner V, Burridge DM (1983) An internal symmetric computational instability. Q J R Meteorol Soc 109:417-428

Houtekamer, P. L., and H. L. Mitchell, 2001: A Sequential Ensemble Kalman Filter for Atmospheric Data Assimilation. Monthly Weather Review: Vol. 129, No. 1, pp. 123-137.

Hunke E.C, Dukowicz J.K. , 1997: An elastic-viscous-plastic model for sea ice dynamics, J. Phys. Oceanogr. 27, 1849–1867.

Hunke E.C., and W. H. Lipscomb, 2010: CICE: the Los Alamos sea ice model documentation and software user's manual version 4.1, Tech. Rep. LA-CC-06-012, Los Alamos National Laboratory.

Hunke, E.C., 2011: Viscous-plastic sea ice dynamics with the EVP model: linearization issues, J. Comput. Phys. 170, 18–38.

W. D. Hibler, A dynamic thermodynamic sea ice model, J. Phys. Oceanogr. 9 (1979) 815–846.

Kundu P. K. and I. M. Cohen, 2004. Fluid Mechanics, 3nd Edition, Academic Press.

Large WG, S.G. Yeager, 2004: Diurnal to decadal global forcing for ocean and sea-ice models: The data sets and flux climatologies. Technical Report TN-460+STR, NCAR, 105pp.

Lellouche, J-M., et al. 2013: Evaluation of global monitoring and forecasting systems at Mercator Océan. Ocean Science 9, 57-81.

Lipscomb, W. H. , E. C. Hunke, W. Maslowski, and J. Jakacki, 2007: Ridging, strength, and stability in high-resolution sea ice models, J. Geophys. Res. 112 (C03S91), DOI:10.1029/2005JC003355.

Olbers, D., J. Willebrand, and C. Eden, 2012. Ocean Dynamics, Berlin, Springer Verlag Berlin, 704 p., ISBN: 978-3-642-23449-1. hdl:10013/epic.39446

Madec, G, P. Delecluse, M. Imbard, and C. Levy, 1998: OPA 8.1 general circulation model reference manual. Notes de l'IPSL, University P. et M. Curie, B102 T15-E5, Paris, No. 11, p91.

Madec, G., 2008: NEMO reference manual, ocean dynamics component: NEMO-OPA. Preliminary version. Note du Pole de modélisation, Institut Pierre-Simon Laplace (IPSL), France, No 27 ISSN No 1288-1619.

Mertens, C., M. Rhein, M. Walter, C. W. Boning, E. Behrens, D. Kieke, R. Steinfeldt, and U. Stober (2014), Circulation and transports in the Newfoundland Basin, western subpolar North Atlantic, J. Geophys. Res. Oceans, 119, 7772–7793, doi:10.1002/2014JC010019

Large, W. G., and S. Yeager. 2004. Diurnal to decadal global forcing for ocean and sea-ice models: the data sets and flux climatologies. CGD Division of the National Center for Atmospheric Research, NCAR Technical Note: NCAR/TN-460+STR

Oke, P.R., P. Sakov and S. P. Corney, 2006: Impact of localisation in the EnKF and EnOI: experiments with a small model, Ocean Dynamics, DOI 10.1007/s10236-006-0088-8.

Penduff, T., J. Le Sommer, B. Barnier, A.-M. Treguier, J.-M. Molines, and G. Madec 2007: Influence of numerical schemes on current-topography interactions in 1/4° global ocean simulations. Ocean Science, 3, 509-524.

Penduff, T., M. Juza, L. Brodeau, G. C. Smith, B. Barnier, J. M. Molines, and A.-M. Treguier, 2010: Impact of global ocean model resolution on sea-level variability with emphasis on interannual time scales. Ocean Science, 6(1), 269-284.

Petrie, B., and J. Buckley (1996), Volume and freshwater transport of the Labrador Current in Flemish Pass, J. Geophys. Res., 101(C12), 28335–28342, doi:10.1029/96JC02779.

Pham D. T., J. Verron and M. C. Roubaud, 1998: A singular evolutive extended Kalman filter for data assimilation in oceanography, J. Mar.Syst., 16, 323-340.

D. A. Rothrock, 1975: The Energetics of the Plastic Deformation of Pack Ice by Ridging, Journal of Geophysical Research 80 (33), 4514– 4519.

Rio, M.-H., and F. Hernandez, 2004: A mean dynamic topography computed over the world ocean from altimetry, in situ measurements and a geoid model, J. Geophys. Res., 109, C12032, doi:10.1029/2003JC002226.

Roullet, G., and G. Madec, 2000: Salt conservation, free surface, and varying levels: a new formulation for ocean general circulation models, J. Geophys. Res., 105, 23927–23942.

Roy F., M. Chevallier, G. C. Smith, F. Dupont, G. Garric, J.-F. Lemieux, Y. Lu and F. Davidson: Arctic sea ice and freshwater sensitivity to the treatment of the atmosphere-ice-ocean surface layer. J. Geophys. Res., in review.

Ryan, A. G., Regnier, C., Divakaran, P., Spindler, T., Mehra, A., Hernandez, F., Smith, G. C., Liu, Y., and Davidson, F.: GODAE OceanView Class 4 forecast verification framework: Global ocean inter-comparison. *J. Operational Oceanogr.*, accepted.

Sandwell, D. T., R. D. Müller, W. H. F. Smith, E. Garcia, R. Francis, New global marine gravity model from CryoSat-2 and Jason-1 reveals buried tectonic structure, Science, Vol. 346, no. 6205, pp. 65-67, doi: 10.1126/science.1258213, 2014.

Schiller A, M Bell, G Brassington, P Brasseur, R Barciela, P De Mey, E Dombrowsky, M Gehlen, F Hernandez, , V Kourafalou, G Larnicol, P-Y Le Traon, M Martin, P Oke, G C Smith, N Smith, H

Tolman, K Wilmer-Becker, 2014: Synthesis of New Scientific Challenges for GODAE Oceanview**. ,** *J. Operational Oceanogr, conditionally accepted.*

Smith G.C., F. Roy, P. Mann, F. Dupont, B. Brasnett, J.-F. Lemieux, S. Laroche and S. Bélair, 2013a: A new atmospheric dataset for forcing ice–ocean models: Evaluation of reforecasts using the Canadian global deterministic prediction system, *Quart. J. Roy. Met. Soc.*, doi: 10.1002/qj.2194.

Smith, G.C., F Roy, J-M Belanger, F Dupont, J-F Lemieux, C Beaudoin, P Pellerin, Y Lu, F Davidson, and H Ritchie, 2013b: Small-scale ice-ocean-wave processes and their impact on coupled environmental polar prediction, Proceedings of the ECMWF-WWRP/THORPEX Polar Prediction Workshop, 24-27 June 2013, ECMWF Reading, UK.

Smith, G.C., F. Roy, M. Reszka, D. Surcel Colan, Z. He, D. Deacu, J.-M. Belanger, S. Skachko, Y. Liu, F. Dupont, J.-F. Lemieux, C. Beaudoin, B. Tranchant, M. Drévillon, G. Garric, C.-E. Testut, J.-M. Lellouche, P. Pellerin, H. Ritchie, Y. Lu, F. Davidson, M. Buehner, M. Lajoie and A. Caya: Sea ice Forecast Verification in the Canadian Global Ice Ocean Prediction System. *Quart. J. Roy. Met. Soc.*, doi: 10.1002/qj.2555.

M. Steele, 1992: Sea ice melting and floe geometry in a simple ice-ocean model, J. Geophys. Res. 97 (C11), 17729–17738.

Testut, C.E. , 2000 : Assimilation de données satellitaires avec un filtre de Kalman de rang réduit dans un modèle aux équations primitives de l'océan Atlantique, Thèse de doctorat de l'université Joseph Fourier- Grenoble 1.

Testut, C.-E., et al., 2003: Assimilation of sea-surface temperature and altimetric observations during 1992-1993 into an eddy-permitting primitive equation model of the North Atlantic Ocean, Journal of Marine Systems, 40-41, 291-316.

Tranchant, B. and M. Drevillon, 2009: SAM2: Système d'Assimilation Mercator #2 Reference Manual. Mercator-Ocean Technical Documentation, pp. 91.

Umlauf L, Burchard H (2003) A generic length-scale equation for geophysical turbulence models. J Mar Res 61:235–265.

Thompson, K.R., Wright, D.G., Lu, Y. and Demirov, E., 2006. A simple method for reducing seasonal bias and drift in eddy resolving ocean models. Ocean Modelling, 13(2), pp.109-125.

M. Van Woert, C. Zou, W. Meier, P. Hovey, R. Preller, P. Posey, 2004: Forecast Verification of the Polar Ice Prediction System (PIPS) Sea Ice Concentration Fields, Journal of Atmospheric and Oceanic Technology 21 (6), 944–957.

Zhai L., Y. Lu, S. Higginson, F. Davidson, F. Dupont, F. Roy, J. Chanut, and G. C. Smith (2015). High-resolution modeling of the mean flow and meso-scale eddy variability around the Grand Banks of Newfoundland. Ocean Dynamics, (DOI) 10.1007/s10236-015-0839-5.